Design of Stent Expansion Mechanisms

by

Graeham Rees Douglas,

B.A.Sc., The University of British Columbia, 2010

A THESIS SUBMITTED IN PARTIAL FULFILLMENT OF
THE REQUIREMENTS FOR THE DEGREE OF

MASTER OF APPLIED SCIENCE

in

The Faculty of Graduate Studies

(Biomedical Engineering)

THE UNIVERSITY OF BRITISH COLUMBIA

(Vancouver)

April 2012

Abstract

Stents are widely used in the treatment of vascular disease and they represent one of the most valuable medical device markets. It has been observed that the mechanical characteristics of a stent influences clinical outcomes.

This thesis is concerned with the design of expansion mechanisms of balloon expandable stents based on the principles of lattice mechanics. Balloon expandable vascular stents are mesh-like, tubular structures used mainly to prop open narrowed arteries, and also to provide sealing and anchorage in a stent-graft for treatment of aneurysms or dissections. Presence of a spatially repeating geometric pattern of a 'unit' or a cell is a striking feature of stents. Lattice mechanics deals with such spatially periodic materials and structures.

The focus is on the plastic expansion phase of a stent from the initial crimped configuration. The elastic post-expansion phase is also considered. Eight unit cell-based stent designs are selected for this work. Their expansion characteristics are analyzed and measured. Analytical methods based on kinematics of stent expansion mechanisms are presented first which are then validated with more detailed Finite Element (FE) calculations. Analytical methods developed in this work aid rapid design calculations in selecting appropriate unit cell geometries. Three of the designs are manufactured through laser micromachining and tested for their expansion characteristics.

The analytical methods were validated as they predicted similar expansion characteristics as finite element and experiment. Additionally, the study confirmed that stent designs with positive, negative, or zero axial strain over expansion is possible. Finally, the study suggest that unit cell design can be tailored to obtain desired length-diameter and pressure-diameter characteristics over the expansion phase of stenting.

Table of Contents

Appendix

List of Tables

List of Figures

List of Symbols

D	Diameter of a stent
L	Length of a stent
δ_c	Circumferential expansion of a unit celll
$\delta_{c,t}$	Circumferential expansion of a stent
δ_a	Axial change in length of a unit cell
l	Length of a stent strut
t	Thickness of a stent strut
w	Width of a stent strut, or stent tube thickness
θ	Angle of rotation of a stent strut
n_c	Number of unit cells in circumferential direction of stent
n_a	Number of unit cells in axial direction of stent
r	Plastic radius of curvature for a bending stent strut
l'	Length of a stent strut, less bending and connecting zones
ψ_0	Angle of the deflected, rigid portion of the Reid-Reddy cantilever
ϕ_1	Angle input parameter for elliptical integrals
a	Length of the rigid zone of a Reid-Reddy cantilever
b	Dimensionless ratio of geometric and material properties
p	Array used to solve the Reid-Reddy cantilever equations
I	Area moment of inertia
E_p	Linear plastic modulus
M_o	Moment causing yield
σ_o	Yield stress
F	Cantilever force
F_o	Cantilever force causing first yield
λ	Ratio of cantilever force to yielding force

u	Cantilever foreshortening at plastic-rigid transition
v	Cantilever deflection at plastic-rigid transition
U	Cantilever foreshortening at end tip
V	Cantilever deflection at end tip
D_o	Initial, unexpanded stent diameter
L_o	Initial, unexpanded stent length
D_1	Stent diameter at a given stage of expansion
D_2	Stent diameter at the next stage of expansion
P_1	Expansion pressure at a given stage of expansion
P_2	Expansion pressure at the next stage of expansion
C	Stent compliance
D_m	Stent diameter at maximum expansion
D_d	Stent diameter at diastole, after expansion
R	Stent recoil
L_d	Stent length at diastole, after expansion
L_s	Stent length at systole, after expansion
f	Stent foreshortening from physiologic pressure changes

Acknowledgments

Thanks to my supervisor Dr. Srikanth Phani for taking a chance on me, years of guidance and knowledge, and patience with my wandering into side projects.

Also thanks to my co-supervisor, Dr. Joël Gagnon for his clinical perspective, encouragement, design feedback, and providing sample medical devices. The project would not have been possible without his knowledge and support.

I have received invaluable feedback and knowledge from Dr. York Hsiang, Dr. Robert Guidoin, Mr. Markus Fengler, and others during my MASc degree. I have been fortunate to have many great teachers, I am thankful for all of them.

I am grateful for the funding that allowed this work, which was provided by the Natural Sciences and Engineering Research Council (NSERC), the Department of Vascular Surgery at Vancouver General Hospital (Dr. Jerry Chen), the Department of Mechanical Engineering at the University of British Columbia, and the Mr. Paul Geyer Graduate Award in Biomedical Engineering.

Dedication

To my parents, who have supported me selflessly, been among my best teachers, and have provided great inspiration.

Chapter 1

Introduction

1.1 Background on Stenting

Stents are medical devices used to hold open various lumens within the body, often fluid-carrying vessels. In the arterial system, stents typically take the form of a tubular mesh-like structure. Arterial stents are used to open stenosed arteries through angioplasty or in anchoring a stent-graft to treat an aneurysm or dissection.

The mesh-like stent can be viewed as a lattice, where a geometric unit cell is repeated in the circumferential and axial directions of the stent to form the device. In lattice materials, the properties of the unit cell have been shown to dictate the effective macroscopic properties of the macrosctucture [1, 2] . Thus, a rational starting point in stent design would be the selection of a unit cell with desirable properties. This analysis focuses on the expansion phase of stenting, which links to the earlier work in our group on the post-deployed mechanics of stents [3].

Anatomy, physiology, disease, and endovascular surgery will first be described to serve as a general background and set the context for stent design.

1.1.1 Anatomy and Physiology

Before designing stents, the anatomy and physiology of the artery should be considered such that the design of the device can account for properties and constraints resulting from the tissue. For this thesis, stents are sized for the aorta, so discussion will focus on this artery. The designs and the paradigms behind these designs are generally scalable to smaller vessels.

Gross Anatomy of the Aorta

The aorta is the largest artery in the peripheral vascular system, spanning a length of 50-70 cm with a diameter of 2.5-3.5 cm [4] (see Figure 1.1). The aorta tapers along its length, and widens by approximately one millimeter per ten years of age in healthy adults. It rises from the left ventricle, then arches anteriorly (towards the front chest wall) and cranially (towards the head), before turning posteriorly (towards the rear chest wall) and caudally (away from the head). It descends parallel to the spine until the bifurcation in the mid-abdomen to the iliac arteries. Commonly, the aorta is described by four anatomical sections: the ascending aorta, the aortic arch, the descending thoracic aorta, and the abdominal aorta.

The ascending aorta starts at the aortic valve, which divides the aorta from the left ventricle. Just distal to the aortic valve are the coronary artery branches which feed the heart and are infamous for atherosclerosis leading to heart attacks. The ascending aorta is about 5 cm long, and, with the pulmonary trunk, is covered by the visceral pericardium.

Cranial to the ascending aorta is the aortic arch, where the branches to the brachiocephalic trunk, left common carotid artery, and left subclavian arteries are found. These arteries feed the head, brain, and upper extremities. The aorta curves considerably to reverse in direction to a downward flow in this section, although the radius of the curvature is individually variable.

Caudal to the aortic arch is the descending thoracic aorta, often referred to merely as the descending aorta. This section of the aorta is tethered by fascia to the posterior thoracic wall, near the spine. This section of the aorta includes only minor branches serving organs in the thoracic cavity: one right and two left bronchial arteries; nine pairs of intercostal arteries; and the pericardial, esophageal, mediastinal, subcostal, and superior phrenic arteries.

The abdominal aorta is separated from the descending thoracic aorta as it passes through the diaphragm, and continues until the bifurcation to the iliac arteries at the L4 vertebra. The major branches of the abdominal

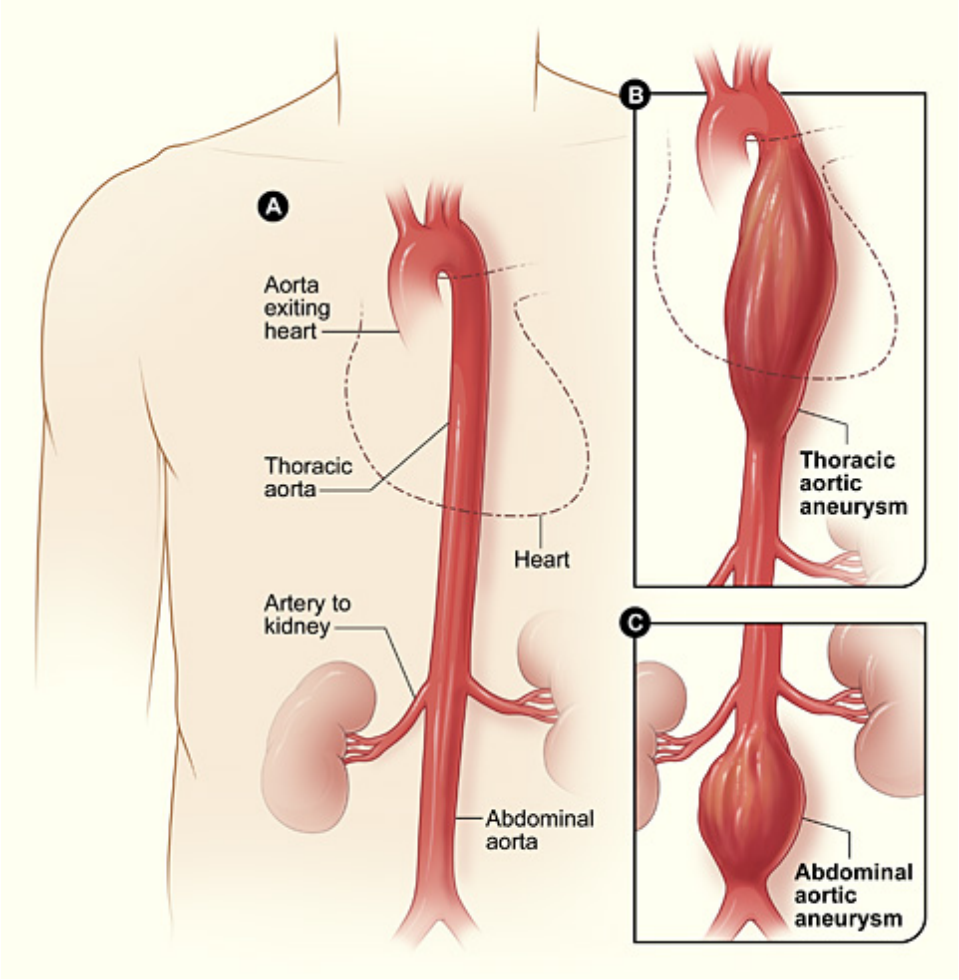

Figure 1.1: The aorta and its branching vessels, with aneurysm examples. Open source image from the National Institutes of Heath, USA

aorta are the celiac axis, servicing the stomach, liver, and spleen; the superior mesenteric artery, servicing the small intestine and proximal colon; the inferior mesenteric artery, servicing the distal colon and rectum; and the pair of renal arteries, servicing the kidneys. Minor branches include the suprarenal, ovarian or testicular, and middle sacral arteries. There are also three sets of paired branches: the inferior phrenic and lumbar arteries.

Layers of the Aorta

The aorta can be viewed as a composite material, consisting of three layers with each layer itself having a heterogeneous structure [4]. Compared to other arteries, the healthy aorta is more elastic; other arteries may be muscular or arterioles, depending on the composition of the middle layer (tunica media) of the artery. The deepest layer of the aorta is the tunica intima, which gives one fifth of the thickness of the aortic wall. A single layer of simple squamous epithelial cells line the inner surface of the intima. It is this thin layer of cells that comes into contact with the blood, and is thought to govern a significant portion of the biological response to implanted devices. Superficial to the epithelial layer is a layer of fibroblasts and macrophages, which are surrounded by an acidic, mucopolysaccaharide-rich extra-cellular matrix, which also contains some elastin.

Superficial to this is the tunica media, the layer giving the aorta its high radial strength and elasticity. It consists of concentric lamellar of elastin; the innermost of these defines the border with the intima and is known as the internal elastic lamina. With age, this border loses definition and is often indistinguishable in elderly age. Each lamellae is separated by a layer of intercellular ground substance, containing thinner strands of elastin, collagen, and undifferentiated smooth muscle cells. The number of layers of lamellae decreases distally: there are approximately 56 layers in the ascending aorta and 26 layers in the abdominal aorta.

The most superficial layer of the aorta is the tunica adventitia, which is a thin, collagen-rich layer containing fibroblasts and some smooth muscle cells. The adventitia also contains the vasa vasorum, which is itself a system of blood vessels, supplying the cells in the artery wall. It consists of small branching arterioles that go from the superficial plexus in the adventitia to the deep plexus in the media. The internal lamellae and the intima do not have deep plexus arterioles, meaning that mass transfer with these cells must first be through the interstitial fluid. The adventitia also contains the nervi vascularis network of the nervous system.

1.1.2 Flow in the Aorta

Before discussing pathology of the aorta that requires the intervention of medical devices, it is worth noting the healthy function to set a contrast with disease, to develop goals for the devices, and to guide in vitro testing of devices. A pulsatile flow is produced in the aorta by the left ventricle [5]. Ventricular contraction induces a pressure wave that travels through the arterial system, followed by a slower wave of fluid translation. The speed of the pressure wave depends on the local stiffness of the artery wall; distally, where the artery is stiffer, the pressure wave propagates faster. The shape of the pressure wave also changes through the arterial system, having a more pronounced systolic phase as it propagates distally.

The propagation of the pressure and velocity waves is not trivial. Proximally, the incursia, or entrance condition arising from the flow through the aortic valve must be considered. In addition to the effect of changing vessel properties mentioned above, further complexity is added by reflection of the pressure waves and damping from viscous tissues both in and surrounding the artery. This reflection is most noted at the site of the renal branches and distal to the iliac bifurcation. These two locations are critical to performance of stent-grafts treating some clinical presentations of Abdominal Aortic Aneurysms (AAA). These locations and other pressure nodes and anti-nodes require Fourier analysis and assumptions of linear response and periodic occurrence in their analysis. The periodic assumption is valid if a subject's heart rate is constant, but the assumption of linearity must be used cautiously as body tissues and even fluids can exhibit highly non-linear behaviors.

Similar to the analysis of the pressure wave propagation, the analysis of the velocity waves propagation is complex and only possible through use of instruments that have only recently become available. The velocity pulse leads the pressure pulse; the flow initially has less resistance in flowing down the artery than in expanding the flexible walls of the artery. Interestingly, backflow exists even in the healthy aorta and femoral arteries. This backflow is seen during the late diastolic phase, and in the center of the vessel. This

creates flattened velocity profiles during the diastole, where shear stresses are concentrated by the walls of the artery. This flow is predominately laminar, but may become turbulent or near turbulent near the left ventricle, more distally at the peak systolic velocity, or if there is a local disturbance or occlusion to the flow. This turbulence or near-turbulence further complicates analysis as it results in a non-linear pressure-flow relation, a greater pressure drop through the turbulent zone, and increased maximum shear rates.

A value named aortic input impedance is given to a frequency-domain metric comparing the pressure and flow pulses. Aortic input impedance is a lumped value giving information about the compliance and dimensions of the downstream arterial network. At high heart rates, impedance is typically less than 2%.

Change in the artery wall can present in several ways. The geometry of the vessel lumen is thought to be at least partially governed by the fluid shear stresses and wall stresses in the artery. This can result in vascular remodeling of the endothelium, or changes in the wall geometry through smooth muscle proliferation. These topics are closely linked with atherosclerosis, both in how they are thought to be formed, and in how they result in the narrowing of the vessel [5]. Aneurysms are another aspect of arterial morphology, the treatment of which is the focus of this thesis. Aneurysms may form in any artery, although they are most common in the aorta. There are there main categories of aneurysm: atherosclerotic, syphilitic, and dissecting.

1.1.3 Arterial Disease: Atherosclerosis and Aneurysms

Atherosclerosis and aneurysms are two diseases that may require stents as part of their treatment protocol. Recent statistics in the United States show that coronary heart disease results in 445 687 deaths a year, accounting for one in five deaths [6]. An estimated 1 255 000 heart attacks occur annually in the United States.

Approximately two million people are estimated to have abdominal aortic aneurysms in the United States, and rupture of these aneurysm are estimated to cause 6 000 to 10 000 deaths annually [7].

Stents are commonly associated with opening coronary vessels narrowed by atherosclerosis. Atherosclerosis, the culprit behind myocardial infarction (commonly referred to as a heart attack), has such a high prevalence in western culture that "its absence in middle life or beyond, not its presence, is noteworthy" (p.89, Lindsay 1994) [8]. Atherosclerotic lesions, commonly referred to as plaques, are lipid-filled smooth muscle cells with a matrix of lipids, collagen, elastin, and proteoglycans. These plaques directly lead to stenosis and reduction of blood flow, and the rupture of this plaque can lead to occlusion of the artery and subsequent myocardial infarction. Risks leading to atherosclerosis are: a history of smoking, diabetes mellitus, hypercholesterolemia, and hypertension. Stents are a common treatment for atherosclerosis, where a stent is used in conjunction with balloon angioplasty to expand the lumen of the vessel, improving flow.

Aneurysm are another common arterial disease. Stents can be used with a fabric tube to make a stent-graft bridging an aneurysm, isolating it from blood pressurization and reducing rupture risk, or as an addition to seal and prevent migration of these devices. The stents considered in this thesis are nominally sized for the aorta, so the aortic pathologies will be discussed in more depth.

Since anatomy ranges widely, it is difficult to categorize what is an aneurysm and what is not. Kent and Boyce suggest that the dilation of the vessel by 1.5 or greater its normal size classifies an aneurysm [9]. This is clearly an arbitrary definition but is included to give some context to the reader. The first successful aneurysm repair was in 1955, and the surgery now has a 2-3% mortality rate for elective surgeries. This is contrasted with a 50-90% mortality rate of a ruptured aneurysm. The unpredictable nature of aneurysm growth and rupture is considered against these statistics, and together they provide motivation for elective aneurysm repair thought to be in danger of rupturing. The risk factors for atherosclerotic aneurysms are the same as for atherosclerosis.

Aortic aneurysms are most common in the infrarenal location in the abdominal aorta just distal to the renal arteries. One theory is that the vasa vasora is less developed here than other aortic locations, resulting in nutrient

deficiency and faster aging of the extracellular lattice that gives the artery its mechanical properties. Another theory is that aneurysms in this location is due to increased stresses or resonance resulting from the node formed from the reflected pressure wave. Yet a third theory is that aneurysms are the result of an enzyme pathology, making it possibly a genetic disease. Arterial tissue of aneurysms are noted for having less and degraded collagen and elastin compared to healthy tissue. Generally this is thought to be the a step in the pathway causing an aneurysm, but some contend that it could instead be a symptom of the aneurysm [9].

Aneurysms can also be caused by other better known pathways. Myotic aneurysms are caused by infections. Connective tissue disease can also cause aneurysms such as Marfan syndrome and Ehlers-Danlos syndrome. These are more often noted in the ascending aorta. The breakdown of the connective tissues weakens the vessel and can lead to aortic dissection, which can be concurrent or independent of an aneurysm.

Syphilitic aortis is the aortic disease resulting from the attack of treponema pallidum bacteria on the vasa vasorum, resulting in damage to the tissue supported by the vasa vasorum [10]. Of patients with syphilitic aortis, 5-10% develop aneurysm, 50% of these are in the ascending aorta, 30-40% are in the aortic arch, 10-15% are in the proximal descending thoracic aorta, and less than 5% are in the abdominal aorta. This counters the typical presentation of aortic aneurysms, which are most commonly found in the abdominal aorta. Untreated, syphilitic aneurysms have a two year mortality rate of 80%.

Aneurysms can also be classified based on the appearance of the vessel weakness. A true aneurysm is a weakness and dilation of the entire vessel, caused by atherosclerosis, medial degeneration, or aortic dissection. This is contrasted with a false aneurysm which has a localized but full-thickness occurrence and allows blood to circulate outside of the artery. These are caused by trauma and infection, and are also referred to as pseudo-aneurysms.

An additional aneurysm classification divides the disease between fusiform and saccular aneurysms. Fusiform aneurysms have a more tapered shape, often from the atherosclerotic version of the disease. Saccular aneurysms,

on the other hand, are more localized and balloon-like. These are also commonly atherosclerotic, as well as syphilitic and myotic versions of the disease.

1.1.4 Stents and Endovascular Surgery

Stenting and endovascular surgery in general were pioneered by Dotter, first reporting on the percutaneous dilation of obstructions in 1964 [11]. Later, Dotter described the implantation of a coil stent in dogs [12] and then in humans [13] to reduce the recoil of the stenosis after the dilator is removed. However, it was not until Palmaz-Schatz's "slotted tube" stent design that the use of stents became widespread [14]. The Palmaz stent continues to be used clinically today, and forms the basis for the "Diamond" stent considered in this thesis.

Endovascular surgery has since grown to become a diverse field encompassing a number of procedures. In general, access to the vascular system is made at a peripheral site, such as the femoral or bracial artery. A variety of tools are used in endovascular surgery, but some essentials are sheaths, guidewires, catheters, imaging devices, and contrast agents [15]. After attaining vascular access, sheaths are used to provide a port to the artery, providing a relatively straight lumen for inserting additional devices as well as a valve preventing excessive bleeding through the access site.

Guidewires are then inserted to provide a "rail" for catheters to follow. Guidewires are easier to maneuver through complex and tortuous anatomy than catheters and can straighten tortuous vessels. Guidance for guidewire positioning is provided by a medical imaging device, most typically flouroscopy. Catheters are then advanced over the guidewires to the target site, also visualized by flouroscopy.

In the case of angioplasty, the catheter is a balloon catheter, where an inflatable balloon is located at the end of the catheter. This balloon applies an expansive force on a stenosis, molding it open. This reduces resistance in the artery, increasing flow. Often, the artery will partially return to a stenosis with balloon angioplasty alone. To prevent this, a

balloon-expandable stent is often used over the angioplasty balloon. The stent plastically deforms around the balloon, forming a scaffold that props the artery open and resists recoil of the plaque/ artery. See Figure 1.2.

Self-expanding stents and stent-grafts are also common endovascular tools. These devices are crimped to greatly reduce their inner lumen and loaded on a catheter. The insertion procedure is similar to balloon-expandable stents, except a mechanism releasing the self-expanding stent is used instead of a balloon to get the device to expand to its final diameter. Accordingly, balloon-expandable stents are typically stiffer and less elastic than self-expanding stents. Conversely, self-expanding stents are more resilient to crushing, for example when used in arteries going through joints where bending of the stent is probable.

1.1.5 Complications of Stenting

Stent use is now widespread although not without complications. Thrombosis, neointimal hyperplasia, and vessel injury are among these complications, and all have been shown to be intimately connected to stent design choice [16]. Thrombosis is due to the clotting action of blood, often in reaction to foreign materials and surfaces. Neointimal hyperplasia refers to tissue growth into the stented lumen. Neointimal hyperplasia is a mid-term complication of stenting, where epithelial and eventually smooth muscle cells migrate. Some groups [3] [17] view the course of neointimal hyperplasia as being largely guided by changes in structural and fluid shear forces. Vessel injury is an acute complication dependent on the mechanics of the implantation procedure.

Thrombosis can be managed with medication, and stents eluting sirolimus or paclitaxel have been made to reduce neointimal hyperplasia. However, recent reports have raised some questions about the lack of improvement to long-term survival and freedom from death and stent thrombosis [18] and very late thrombosis events [19] in drug-eluting stents.

Stent design has been shown to have a prolific impact on thrombosis and neointimal hyperplasia [20] [21] [16], but little study has been preformed on

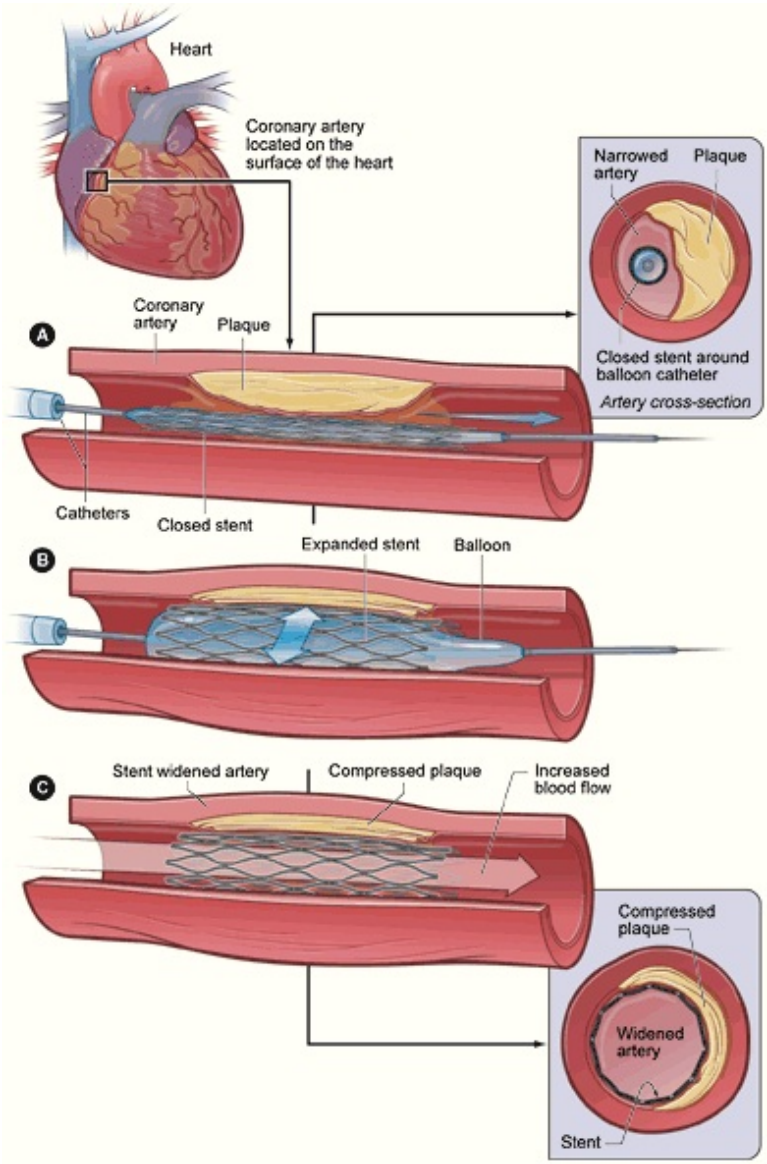

Figure 1.2: A stent, expanded by a balloon, props open a plaque in an artery. Open source image from the National Institutes of Heath, USA

what specific mechanism of design cause these effects.

These findings have provided motivation for the present study into mechanism of stent design.

1.2 Mechanics of Stents

Other groups have studied various mechanical parameters of stenting, often with finite element (FE) or experimental methods. A variety of methods are used to model the balloon, stent, and artery during expansion, in initial contact with the artery, and the long term, cyclic loading the stent experiences *insitu*.

Hara et al. reviewed many stent parameters and the state-of-the-art of stent design in 2005 [22]. The radial flexibility of a stent is important: if the stent is too elastic, it will recoil when the balloon is deflated, resulting in reduced lumen gain. For example, coiled stents have less lumen gain and higher late loss than tubular and corrugated designs. Corrugated designs have been shown to have lower neointimal hyperplasia than a slotted tube (Palmaz-Schatz) design in animal trials. Hara et al. also reported that stents that deploy with a more circular cross section appear to have larger late lumens. In the same review, materials and coatings are discussed. Covered stents have been tried but were not found to reduce restenosis. Biodegradable stents had been proposed to reduce restenosis, and recently (2011), the Abbott Absorb bioresorbable stent has been approved in some jurisdictions. Thinner struts were recommended to reduce restenosis and re-intervention rates. For stent coatings, gold appears to increase restenosis and platelet formation; silicon carbide showed no significant difference over bare metal; heparin reduced thrombosis and smooth muscle cell migration and proliferation in some studies, but randomized trials showed no impact of the coating. Drug-eluting coatings, which are essentially locally toxic drugs disrupting the cell cycles of nearby cells, have been virtually proven to reduce restenosis but not eliminate it. One stent design parameter is if the unit cell used is a “closed cell” or “open cell”. Closed cell designs have a higher strut density. Open cell designs have a lower strut density by removing selected

struts in the stent's lattice. Closed cell stent designs provide better drug distribution than open cell designs, but have reduced flexibility. In practice, this becomes even more complicated as stents rarely expand into smooth, straight arteries. Thus, relative positioning of struts within a stent can vary in different patients for the same stent design.

Moore et al. reviewed the effect of stent design on hemodynamic and arterial wall stress [23]. Flow disruption is a key issue with stent design. The manufacture of a stent makes struts that inherently cause backward and forward facing steps in the wall condition of the flow. These steps cause local stagnation points (low fluid shear stress), which have been shown to lead to tissue growth. Large spaces axially between struts have been found to be important; too short of spacing and the periodic stagnation zones combine into a continuous stagnant layer, particularly in smaller stents such as those for the coronary arteries. Shear stress has been shown to promote endothelial cell migration. High stress may cause platelet activation and thrombosis. Solid mechanics based stress on tissue from the stent was also reviewed by Moore et al. Both stresses from acute expansion as well as long term stresses from the blood pressure cycle likely impact outcomes of stenting. The review included several sources providing evidence that arteries grow and thicken in response to stress concentrations and low wall shear stresses.

Probably the most rigorous simulation of stent-artery interaction was preformed by Holzapfel et al [24]. The geometry of an external iliac artery harvested post-mortem from a 65 year old woman was extracted using hrMRI. Non-linear material models were then applied to six different layers of the artery-plaque model. The Multi-Link Tetra (Guidant, now Boston Scientific), NOROYAL-elite (Boston Scientific), and InFlow Gold Flex (In-Flow Dynamics, now Boston Scientific) were considered as parameterized base unit cell designs. The lengths, thicknesses, and radius of curvature of various struts within these stents were then manipulated for comparison. The stent is expanded through displacement boundary conditions applied to the inner surface of the stent and a physiologic blood pressure is applied to the artery. One parameter the study examined was the effect of stent

design on arterial stress for different ratios of mismatch between the lumen of the unstented artery and the expanded lumen. Larger mismatches cause different levels of stress for different stent designs. Stent unit cell geometry was found to have one of the largest effects on the resultant stress state. Reducing strut thickness was also shown to be a contributing factor, but to a lesser degree.

Tan et al studied the Palmaz-Schatz (Cordis) and Freedom (Global Therapeutics, now Cook) stent geometries using finite element, looking at the effects of changing strut thickness, number of struts circumferentially, and plaque stiffness to compare the two stent designs [25]. They also proposed an analytical model of expansion for the Freedom stent and qualitatively described the expansion of the stents as being plastic hinges. They found that the Palmaz-Schatz stent had a more distributed plastic hinge zone, and therefore this stent would be less likely to have strut fracture and is less limited in its expansion diameter. However, the Freedom stent was found to be more axially flexible. Axial flexibility lets stents fit better in curved arteries and tract through more tortuous anatomy during delivery of the stent to the target lesion.

The plastic hinge model of strut expansion was also mentioned by Charalambides in his thesis [26]. The Taxus (Boston Scientific) stent was modeled with variation of some parameters for comparison, and the balloon and artery were included in some parts of the analysis. Abaqus CAE (Standard) was used for the analysis, using the Ramberg-Osgood material model. In part of the analysis, single struts are modeled as being representative of the entire structure. The width and thickness of the strut are varied to determine the contribution of each to the stress concentrations resulting from expansion. An analytical expression for stent expansion as a function of stent strut angle is presented for this particular geometry assuming a plastic hinge. Loading for stent expansion analysis was provided by applying a pressure of 20 N/mm^2 to the inner surface of the stent.

An analytical model along with FE analysis on woven stents (for example, the Wallstent (Boston Scientific) was developed by Zahora [27]. Few analytical models exist for corrugated and slotted tube-style stent designs.

The S7 (Medtronic) and NIR (Boston Scientific) stents were compared through FE by Lally et al. [28]. The expansion phase was not considered, instead stents of an assumed expanded geometry were placed in an stretched artery, then the stretching forces were removed allowing the artery to recoil around the stent. The inner surface of the stent was then loaded with systolic-equivalent pressure. The authors found that the NIR stent had higher stress concentrations, and commented that this matches clinical findings that the NIR stent has nearly twice the reported restenosis rate at a six month follow up.

A finite element-based parametric study of stents based on the corrugated ring design was reported by Bedoya et al [29]. Strut spacing, radius of curvature, amplitude of corrugation, and arterial area coverage were varied. The stent was modeled in an expanded state from an assumed geometry. The artery was then stretched, and finally allowed to recoil around the stent. The study predicted that axial corrugation spacing has the greatest impact on arterial stress, with broadly spaced rings having reduced arterial stress. Increasing the amplitude of the corrugations and avoiding sharp corners are also predicted to be beneficial to reduce stress imposed on the artery.

Radial stent-artery compliance mismatch was described by Berry et al., who proposed a stent design reducing this mismatch particularly in the ends of the stent [17]. Their Compliance Matching Stent (CMS) is compared to a shorter Palmaz-Schatz stent through FE and in vivo hemodynamic analysis in a swine model. The CMS was found to have a more distributed stress profile, with a three to five times reduction in peak circumferential stress.

Petrini et al. also considered axial flexibility of stents using FE by imposing rotations about orthogonal axis at the ends of the stent [30]. The study considered the BX Velocity (Cordis) and Sirus (Carbosent) stents in their crimped and expanded configurations. The major design difference between the two stent designs is the degree of and configuration of a corrugated strut that axially links coils of circumferentially running struts. The BX Velocity stent was found to have a greater axial flexibility.

Mori et al. used FE and experiments to compare axial flexibility of stents using four point bending and uniform moment bending methods [31]. The

authors discouraged the use of a cantilever method of fixing one end of the stent and loading the opposite as it does not result in a representative or even distribution of stresses along the specimen. The study compared four different flexure designs of struts axially connecting coils of circumferentially running struts. They found that design is highly important for stent flexibility, although highly flexible designs might have poor patency. Their most flexible design was seen to have localized kinking, which also resulted in a reduced and non-circular lumen.

Balloon design also plays a pivotal role in stent mechanics. Ju et al. preformed a finite element study of Palmaz-Schatz expansion with balloons of different lengths [32]. The study reported that over-length balloons result in the appearance of dogboning, or end-flair, in the stent. Using under-length balloons, the opposite effect is seen and the ends of the stent are under expanded. Ju et al. also demonstrated the use of symmetry in a stent to model only a portion of the stent, reducing computational requirement.

Wang et al. also studied the effect of balloon geometries on the expansion of two stent designs in FE and under digital camera observation [33]. One of these stent designs has the interesting and useful property of having near-zero foreshortening with radial expansion due to a "v-shaped connector" between circumferentially running rings of the stent. The study found that stent geometry and balloon geometry both contribute to the "dogbone" flaring phenomenon.

Beule et al. simulated the expansion of a Cypher (Cordis) stent using different models for the balloon [34]. Many previous studies have used pressure applied to the inner surface of the stent or a smooth balloon model that expands the stent. Beule et al. simulated these conditions as well as a model of a folded balloon, which is more representative of the reality. The folded and unfolded balloon models produced quite similar results, but applying pressure directly to the inner surface was found to deviate somewhat from these.

In vivo examination of neointimal hyperplasia by intravascular ultrasound (IVUS) was reported by Hoffmann et al. [35] . They found the Multi-Link stent (Guidant, now Boston Scientific) had the lowest neoin-

timal hyperplasia of four stent designs. Recall the Multi-Link stent is a near zero-foreshortening design. The Palmaz-Schatz (Cordis) stent had the second lowest neointimal hyperplasia, followed by the NIR stent (Boston Scientific), and then the InFlow stent (InFlow Dynamics, now Boston Scientific).

Sick et al. also reported human, in vivo follow up of restenosis with the Micro II (AVE, now Medtronic), Sito (Sitomed), Pura Vario (Deven Medical), and InFlow stents [36]. Some of these designs have near-zero foreshortening, some do not. Strut thickness varies between design. In contrast to Hoffmann et al., this study found no significant difference in restenosis or adverse events at a six month follow up in a study of 925 patients.

Yoshitomi et al. randomly assigned one hundred coronary stenting patients either a Multi-Link or GFX (AVE, now Medtronic) stent [37]. On four month follow up by IVUS, the Multi-Link stent patients were found to have a larger minimal lumen in the stented artery and a four percent restenosis rate. The GFX stent had a twenty-six percent restenosis rate. The authors noted several differences in the mechanical designs of the two stents; Multi-Link struts have half the thickness, a lower metallic surface area, and a different unit cell design.

A swine in vivo model was studied by Sullivan et al. to compare the Palmaz-Schatz stent with a novel design [38]. The novel design intentionally had thicker struts and sharper corners to induce higher stresses. The authors found a statistically significantly higher restenosis rate and a higher rate of vascular injury (defined as fracture of the internal elastic lamina). A correlation was found between injury severity and neoinitmal hyperplasia thickness. From the results of the study, stent designs with low-profile struts and geometries were recommended to reduce local stress concentrations.

As can be seen from the presented literature, there are many competing design parameters involved in the design of stents. However, relatively little focus has been given to the unit cell geometry used in the stent's design, which is surprising since this parameter has one of the highest impact on the stent's mechanics. Our group has previously studied the effect of unit cell

geometry on stent mechanics using finite element analysis on stents under blood pressure loading [3]. This study controlled parameters except unit cell geometry. The primary findings of this study was that stent architecture can be designed to make stents that shrink, stay constant, or elongate axially when expanded radially, and that unit cell design has a large impact on the radial compliance of the stent. For this study, only blood pressure loading directly on the stent is considered, and the boundary conditions are not representative of reality. The stents are modeled as assumed expanded geometries, and thus have idealized geometries and do not account for material properties changes due to manufacturing or plastic expansion.

The purpose of this thesis is to extend previous work on lattice-inspired stent design to include the expansion/ deployment phase of stent mechanics modeling.

1.3 Lattice Mechanics

In addition to prior work on stents, an introduction of lattices and their analysis is needed to provide background for this thesis. Stents can be viewed in some ways as 2D lattices using a cylindrical coordinate system, although they are loaded and expand plastically in the third (radial) dimension. Most of the literature focuses on 2D planar geometry loaded within the linear range, although plastic deformations have also been considered [39] [1].

Early work on this topic was summarized in a two volume book by Baker, outlining analysis of elastic and plastic structures starting before and continuing through the Second World War [39]. An early application of this theory was used to design bomb shelters capable of protecting occupants from blasts by absorbing energy through plastic deformation.

Prior to this and related work, the previous paradigm was that structures' yield points were considered their failure points. However, structures can survive beyond yield and may be required to in order to perform their desired function. Stents, for example, require a large plastic strain (typically 100-500%) to function. Baker presented analysis that is now standard for bending loading, with a lesser shear component. While Baker focused his

analysis on deformable structures, typically box-like in design, the analysis is analogous to the unit cell analysis of a lattice structure.

Such unit cell analysis was reported by Gibson et al. for a planar, 2D hexagonal honeycomb [1]. Elastic strain, plastic collapse, elastic bucking, and fracture are considered modes of response to loading. Parametric equations for relative density, effective modulus, and Poisson ratio in two perpendicular vectors for linear elastic, elastic buckling, and plastic deformation. A unit cell is taken to be a minimum structure that, when spatially repeated, forms an entire structure. The unit cell is then further reduced and analyzed by symmetry. The resulting analysis is of single struts of the unit cell, with factors accounting for the geometric arrangement of the struts within the unit cell and the relative direction of applied stress. The plastic analysis is for compressive loading; it will be repeated in this thesis under tensile (expansive) loading for the consideration of stent expansion.

Other techniques exist for predicting effective material properties of lattices, such as by using wave propagation through lattices to predict linear material properties in planar, 2D geometries [40] [2]. Using this approach, Chopra considered thirteen unit cell designs, however only six of these are appropriate for stenting since they can undergo large strains needed for stent crimping and expansion. These six, having radial strain potential, will be combined with additional lattice-based stent designs for consideration in this thesis.

1.4 Research Objectives and Outline

Following from the literature review, three objectives are identified for this thesis, which will be covered in subsequent chapters:

1. Develop analytical models to efficiently and reliably predict expansion behavior of stents.
2. Design geometries with desired expansion characteristics based on the developed model.
3. Validate the modelling approaches.

In studying these, the major performance parameters that will be considered are maximum expansion diameter, axial strain, compliance, and recoil. Maximum expanded diameter is a metric describing the packing efficiency of a stent design. It is important for larger vessels so that a stent for a large target vessel can be initially narrow to cause less damage while navigating arteries. Axial strain is an important parameter for two primary reasons. In small vessels, large axial strain contributes to the stress state in the arterial tissue, which could produce remodeling forces and subsequent lumen reduction. In large vessels, large axial strains through expansion cause the stent position to shift significantly, making precise placement difficult. Compliance is important because low compliance could make expansion of the balloon difficult and risk balloon rupture. Post-expansion compliance contributes to the stress state in the artery, and an overly compliant stent may be unable to prop the artery. Recoil of the stent after the expansion balloon is deflated is important since large recoils will result in a reduction in lumen.

Chapter 2 presents two analytical models to quickly predict stent expansion behavior, with the design iteration cycle being under one second. A model based on kinematic analysis of expansion is first presented, followed by one utilizing a plastic cantilever bending model derived from the literature [39]. This cantilever based method has the further advantage of containing information about the relative stiffness of the structure.

Chapter 3 considers the plastic expansion and post-expansion phases of stenting using finite element analysis (FE). FE provides validation for the analytical models, as well as providing additional information about the expansion, including stress distribution within the stent. The recoil after expansion and mechanics under loading from the blood pressure cycle are also modeled. However, the design cycle time using the finite element (FE) approach is approximately one day per design.

Chapter 4 describes experiments that were undertaken to expand stent prototypes. It provides validation for the mechanism of expansion models from both the analytical and FE methods. However, kinetics involved were not measured, and strains present from blood pressure-equivalent loading are too small to accurately measure by the techniques used. The design

iteration cycle for testing prototyped stents could be as low as one week, but was more typically over a month due to manufacturing lead times.

Chapter 5 contains the conclusions and future work of this thesis. Early work on a proposed method to determine stent compliance through expansion analytically is presented here as a direction for future work.

Chapter 2

Analysis of Stent Expansion

2.1 Introduction

Balloon expanded stents are cut in a crimped orientation from a hollow metal tube, with a design intended to expand radially by inflation of an angioplasty balloon. This expansion is plastic, and designed to apply a radially outward force on the artery to open a stenosis and avoid migration of the device. This expansion can be modeled through analytical methods to provide insight into stent design and allow rapid simulation of stent expansion.

Candidate stent designs based on lattice unit cells will be presented. A model based on kinematics of expansion is presented next, along with the results and discussion of this method. A second model based on kinetics of expansion is then presented and discussed. Stent struts in different unit cells have different end conditions. These differences were ignored in the kinematic and kinetic expansion models. To determine the influence of these end conditions on expansion, a FE study on the different mechanisms was undertaken and presented in this chapter. Finally, the limitations and conclusions of these analytical methods will be discussed.

2.2 The Stent as a Lattice

Most stent designs can be viewed as a lattice, wherein a unit cell design is repeated in the axial and circumferential directions of the stent. It has been shown that the mechanics of a unit cell can be analyzed and extrapolated to describe the mechanics of the entire lattice [2] [1]. A unit cell itself is made of struts. In the case of a stent, it is herein assumed that these struts expand in a repeatable way such that analysis of a strut can be expanded

to describe the mechanics of the unit cell. Then, the mechanics of the unit cell can be used to describe the entire stent.

Stent struts in a stents unit cell can be divided into two types: axially running struts that do not bend on expansion, and bending struts which allow the circumference and therefore diameter of the stent to expand under the balloon's contact. From experimental observation of the stents expanded in Chapter 4, plastic bending in the bending struts seems to be confined almost entirely to the ends of the strut. From this observation, the stent expansion is initially analyzed as a rigid mechanism, and later modified with correction terms to account for the non-zero radius of the bend allowing the strut to pivot and to account for material in the stent contributing to connecting struts at the nodes of the stent.

A pin jointed model of stent expansion will be first presented, followed by a modified pin jointed model accounting for the non-zero bend radius of the stent struts. The results of a MATLAB simulation of these models are then presented, and these results are discussed.

An alternative analytical model is then given, expanding on a cantilever bending model developed by Reid and Reddy [41]. This model has the advantage of not requiring an empirical correction factor for the radius of curvature of the stent strut, and is a kinetic method so stiffness properties could theoretically be determined. The expansion results for this model are then presented and discussed.

2.3 Pin Jointed Analytical Model

The geometry of a single cell through stent expansion is considered first in this section. A stent starts as a structure of axially running struts, some of which will bend and some that will not. By assuming that the bending struts bend at the same rate, the bending struts can be modeled as being pin jointed members rotating at the same rate. With this, the entire expansion can be resolved by modeling the struts as rigid members rotating through the same angle, resulting in a given length and diameter for the total structure.

The resulting axial and circumferential displacements of the nodes of the

cell are then multiplied by the number of cells in each of the two respective directions. Loading on the stent is assumed to be entirely radial, which translates into force in the circumferential direction, similar to hoop stress in pressure vessels, but no force in the axial direction. In reality, there will be a component of axial force arising from the interaction between the stent and the balloon, and complex interactions between the stent, balloon, artery, and blood flow. Any changes to the axial length of the stent are therefore assumed to be a result of the effective Poisson ratio of the stent-lattice. The effective Poisson ratio is borrowed from the materials science parameter, where the parameter describes the loading in one direction causing strains in other directions. In the case of a stent, the *effective* macroscopic Poisson ratio is a result of the structure of the stent, rather than a material parameter.

Figure 2.4 illustrates the geometries used in this study. Diamond, Auxetic, and Hexagon are relatively commonly examined designs from lattice literature. The Double Hexagon design examines the effect of removing select axial struts, which would give the stent greater axial flexibility and make it easier to mold into curved arteries. Hybrid designs combine positive and negative effective Poisson ratio sub-units to form a zero-effective Poisson ratio, as shown in Figure 2.2. This principle is used in the design of the Hybrid A and Hybrid C stents. The Chevron unit cell has a zero effective Poisson ratio itself, and is used to create the Chevron A and Chevron B stents.

Two versions of the pin jointed model exist, a pin-jointed and a corrected model. The corrected model includes a non-zero radius of curvature at strut intersections, using an empirically derived correction factor. A unit cell under the crimped, pin-jointed expanded, and corrected-pin-jointed expanded is shown in Figure 2.3 to illustrate the methods.

2.3.1 Diamond

The stent cell is initially modeled as a pin-jointed structure with rigid struts. The horizontal direction in Figure 2.3 corresponds to the axial direction

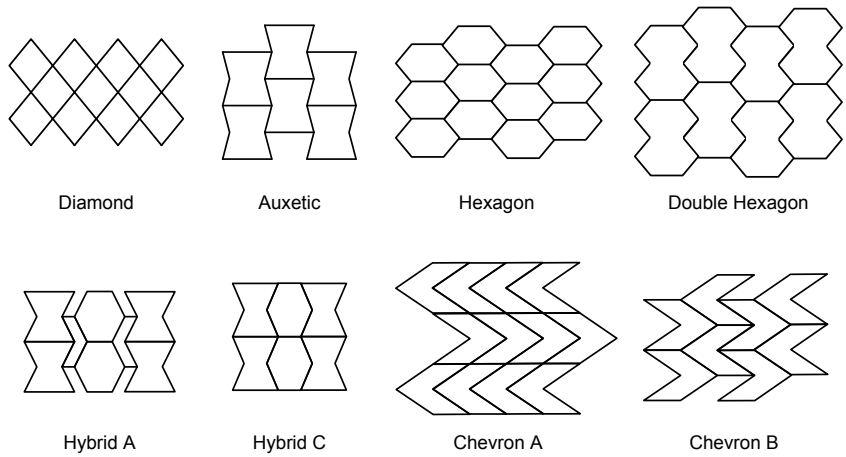

Figure 2.1: Idealized geometries used in this study. The horizontal is the axial direction of the stent and the vertical is rolled to become the circumferential direction.

in the stent, and the vertical direction corresponds to the circumferential direction. The struts that bend to allow the expansion of the stent are referred to as bending struts. The four struts that rotate from the left to centre diagrams in Figure 2.3 are bending struts. For reference, Figure **??** is included to illustrate the parameters used in the subsequent equations. If θ is the angle of the bending struts from the horizontal (symmetrical expansion is assumed), then the displacement in the circumferential direction of the stent with respect to θ is:

$$\delta_c = 2lsin\theta \tag{2.1}$$

where l is the nominal strut length.

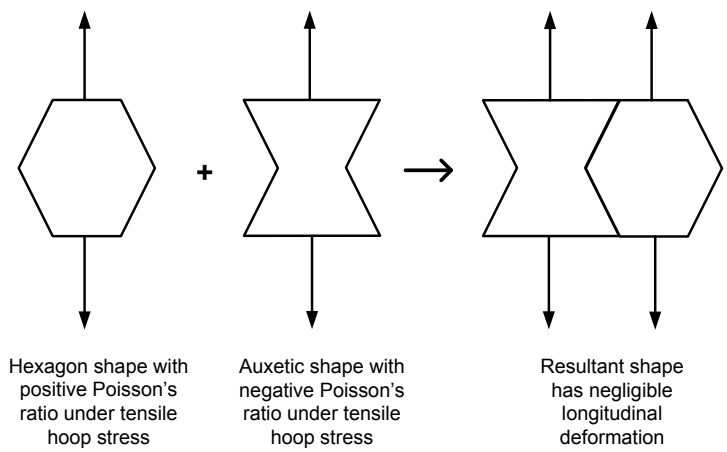

Figure 2.2: Positive and Negative Effective Poisson Ratio Sub-Units are combined to make a combined structure with a zero-effective Poisson ratio.

The total circumferential displacement of the stent is then:

$$\delta_{c,t} = 2n_c l sin\theta \tag{2.2}$$

where n_c is the number of cells in the circumferential direction of the stent. The diameter of the stent, D, at any given stent strut angle, θ, is then the initial diameter, plus $\delta_{c,t}$, divided by π:

$$D = \frac{4tn_c + 2n_c l sin\theta}{\pi} \tag{2.3}$$

where t is the thickness of a stent strut. Similarly, the displacement in the axial direction for a single cell with respect to θ is:

$$\delta_a = -2l cos\theta \tag{2.4}$$

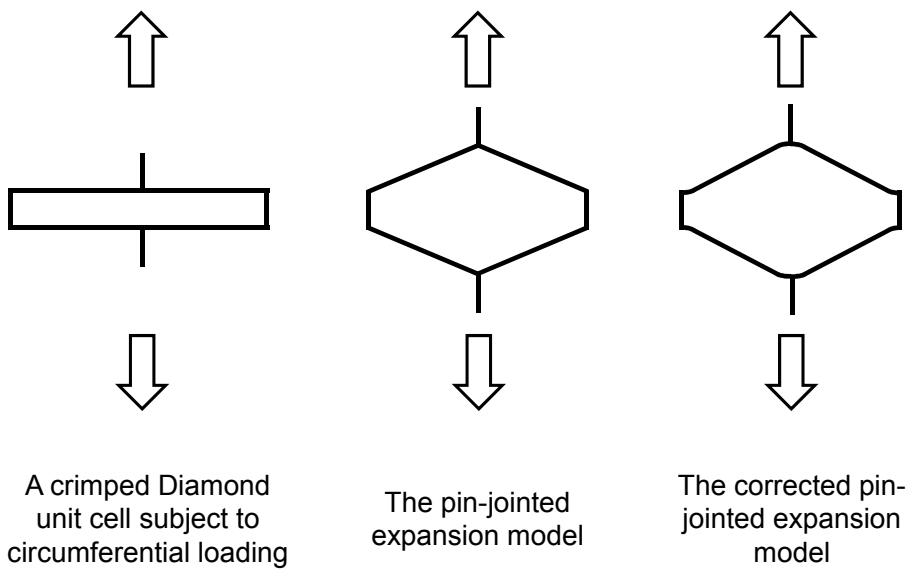

Figure 2.3: A crimped diamond stent (left) subject to a circumferential stretching expands. The pin-jointed jointed expanded cell (centre) and corrected pin-jointed expanded cell (right) are shown for comparison.

Thus, the length of the stent , L, at any given stent strut angle, θ, is:

$$L = 2n_a l cos\theta \tag{2.5}$$

where n_a is the number of cells repeated in the axial direction. The equations for stent diameter and axial length are then simulated in MATLAB for an array of stent strut angles, θ, from 0 to 90 degrees. True stents have connecting struts between bending struts and the bending struts do not pivot but rather bend plastically over non-zero lengths of the strut. Corrective terms are therefore added to the single-cell displacement equations. First,

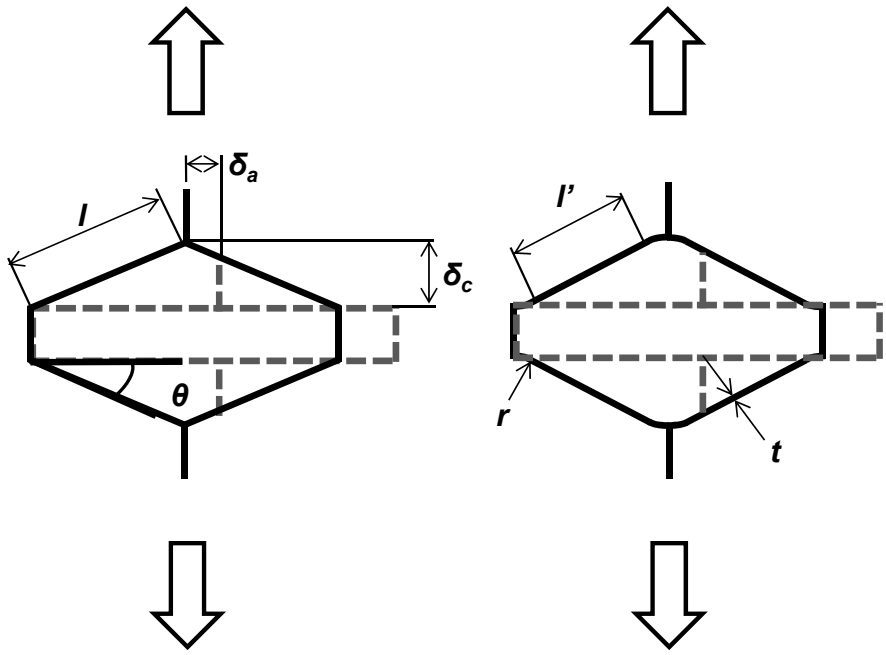

Figure 2.4: Parameters used in the pin jointed analytical formulations are illustrated. Left is the uncorrected pin-jointed model and Right is the corrected model, accounting for the radius of strut curvature, r. Imposed over both images is the crimped geometry, shown with dashed lines.

the strut length is adjusted to include consideration of circumferentially-running struts that link the bending struts together. In Figure 2.3, the circumferentially running struts are the short, straight, and vertical struts. These struts are twice the thickness of other struts in our particular design. Accordingly, the corrected strut length, l', is defined by:

$$l' = l - 2t - \frac{t}{2n_a} \tag{2.6}$$

where the last term represents the connecting strut needed to close the last

cell in the stent's lattice. Thus, the equations for stent diameter and axial length, with respect to stent strut angle, θ, are respectively:

$$D = \frac{4tn_c + 2n_c l' sin\theta}{\pi} \tag{2.7}$$

$$L_{axial} = 2n_a l' cos\theta + t(4n_a + 1) \tag{2.8}$$

A final correction is applied to account for the non-zero bending radius of the strut, r. For simplicity, it is assumed that yielding occurs such that the strut bends with a constant radius, with longer bending regions resulting from greater strut angles. This model appears to match observations of finite element expansion models and experiments, as will be presented in Chapter 3 and Chapter 4 of this thesis. The equations for stent diameter and axial length, with respect to stent strut angle, D, at any stage of the expansion are respectively:

$$D = \frac{4tn_c + 2n_c(l' - 2r\theta)sin\theta}{\pi} + 4rn_c(1 - cos\theta) \tag{2.9}$$

$$L_{axial} = 2n_a(l' - 2r\theta)cos\theta + t(4n_a + 1) + 4rn_a sin\theta \tag{2.10}$$

2.3.2 Auxetic

Auxetic geometry is one of only several known geometries having a positive effective Poisson ratio, and is perhaps the most efficient in terms of being able to undergo significant diametric strain. Similar to the Diamond geometry, the Auxetic geometry analysis gives diameter of the stent as:

$$D = \frac{8tn_c + 2n_c l sin\theta}{\pi} \tag{2.11}$$

for idealized, pin-jointed mechanics.

The strut length for the Auxetic stent is modified by the following:

$$l' = l - 3t - \frac{t}{2n_a} \tag{2.12}$$

resulting in

$$D = \frac{8tn_c + 2n_c(l' - 2r\theta)sin\theta}{\pi} + 4rn_c(1 - cos\theta) \tag{2.13}$$

for the modified case.

Note the only difference compared to the Diamond geometry being the change in the coefficient of the first term, due to manufacturing constraints of the more complex cutting pattern. Accordingly, n_c for an Auxetic stent is one half the value of a Diamond stent if all other parameters are conserved. In general, the number of repeated cells in either direction is not conserved between geometries.

For the length, the analysis now includes axially running struts with projected length that does not change as a function of strut angle. For example, these non-bending struts are illustrated in Figure 2.2 as the horizontal struts in the Auxetic and Hexagon units. Accordingly, the pin-jointed formula for axial length is:

$$L = 2n_a l + 2n_a l(1 - cos\theta) \tag{2.14}$$

and the modified formula

$$L = 2n_a(l' + 3t) + 2n_a(l' - 2r\theta)cos\theta + 4rn_a(\theta - sin\theta) + t \tag{2.15}$$

Note that these equations do not account for bending of the circumferentially

running connecting struts, or a non-uniform bending radius along the length of the strut.

2.3.3 Hexagon

The Hexagon stent is similar to the Diamond stent, except that the circumferentially-running connector strut is extended axially to the same nominal length as the bending struts. Thus, it has the same diameter expansion characteristic as the Diamond geometry:

$$D = \frac{4tn_c + 2n_c l sin\theta}{\pi} \tag{2.16}$$

with the same length correction

$$l' = l - 2t - \frac{t}{2n_a} \tag{2.17}$$

resulting in the modified equation

$$D = \frac{4tn_c + 2n_c(l' - 2r\theta)sin\theta}{\pi} + 4rn_c(1 - cos\theta) \tag{2.18}$$

For length, the pin-jointed model gives

$$L = 2n_a l cos\theta + n_a l \tag{2.19}$$

and for the modified case

$$L = 2n_a(l'r\theta)cos\theta + t(4n_a + 1) + 4rn_a sin\theta + (2n_a - 1)(l' + 2t) \tag{2.20}$$

Note that since Hexagon unit cell results in an open cell at its boundary, an extra set of struts were added to close the last cell. To maintain the same

nominal strut length between stents, the crimped Hexagon stent is therefore one strut length longer than the other geometries. Also note that the non-zero strut widths are taken from the bending struts rather than from the non-bending struts. This was to keep the effective bending strut length the same as the Diamond geometry.

2.3.4 Double Hexagon

The Double Hexagon design is identical to the Hexagon design, except that alternate non-bending struts are removed. By the pin-jointed models, the length and length correction equations for the Double Hexagon design are identical to the Hexagon equations. The diameter expansion characteristic is:

$$D = \frac{8tn_c + 4n_c l sin\theta}{\pi} \tag{2.21}$$

with the modified model giving:

$$D = \frac{8tn_c + 4n_c(l' - 2r\theta)sin\theta}{\pi} + 8rn_c(1 - cos\theta) \tag{2.22}$$

However, noting that n_c for the Double Hexagon design is one half that of the Hexagon design, th results for diameter for the Double Hexagon design are identical to the Hexagon design when using this model.

2.3.5 Hybrid A

For a Hybrid A stent, diameter as a function of strut angle is given by

$$D = \frac{8tn_c + 2n_c l sin\theta}{\pi} \tag{2.23}$$

for the pin-jointed model and for the modified case, the corrected strut length is

$$l' = l - \frac{11}{5}t + \frac{t}{5n_a} \tag{2.24}$$

So the corrected diameter function is

$$D = \frac{8tn_c + 2n_c(l' - 2r\theta)sin\theta}{\pi} + 4rn_c(1 - cos\theta) \tag{2.25}$$

for the modified model.

The length of the stent is described as

$$L = 5n_a l + 2n_a l[(1 - cos\theta) - (1 - cos\theta)] \tag{2.26}$$

or simplified as

$$L = 5n_a l \tag{2.27}$$

and the modified stent length is

$$L = 5n_a\left(l' + \frac{11}{5}t\right) - t \tag{2.28}$$

which is equivalent to the pin-jointed model. Note that all bending struts are designed to have the same length to expand in an even way, and the axial strut in the hexagon has a length of l' to best approximate a regular hexagon.

2.3.6 Hybrid C

The Hybrid C geometry has the same radial expansion mechanism as the Auxetic geometry, except that only six strut thicknesses are required for expansion (n_c is accordingly adjusted). Thus, the diameter as a function of strut angle is:

$$D = \frac{6tn_c + 2n_c l sin\theta}{\pi} \tag{2.29}$$

for idealized, pin-jointed mechanics and when the strut length is corrected by

$$l' = l - \frac{5}{2t} \tag{2.30}$$

the modified expression becomes

$$D = \frac{6tn_c + 2n_c(l' - 2r\theta)sin\theta}{\pi} + 4rn_c(1 - cos\theta) \tag{2.31}$$

Note that the continuous, axially running struts eliminate the need to account for the distribution of a single thickness strut to close the end of the stent. As Hybrid C geometry has continuous axial struts, this analysis predicts no change in length through stent expansion. The length could be described as:

$$L = 4n_a l + 2l \tag{2.32}$$

where the second term is so that both ends of the stent have Auxetic geometry.

2.3.7 Chevron A

Chevron A geometry has the same expansion mechanism as Hybrid C, only alternating bending struts are flipped in orientation to give a chevron pattern instead of a hexagon-auxetic pattern. It also has axially-running struts, which prevent axial strains, as seen in Figure 2.4. Thus, the equations modeling expansion are the same as for Hybrid C.

2.3.8 Chevron B

The Chevron B geometry is derived from the Chevron A cell, where cells orientation is flipped and shifted by half of one cell height each axial column of the stent. Alternatively, the geometry could be described as similar to Hybrid A, where the unit cell is half hexagon, half auxetic instead of alternating hexagon and auxetic cells. Accordingly, the equations for diameter are the same as for Hybrid A, but with the corrected strut length being:

$$l' = l - 3t - \frac{t}{2n_a} \tag{2.33}$$

The length of the stent is described as

$$L = 2n_a l + n_a l[(1 - cos\theta) - (1 - cos\theta)] \tag{2.34}$$

or simplified as

$$L = 2n_a l \tag{2.35}$$

and the stent length is

$$L = 2n_a(l' + 3t) - t \tag{2.36}$$

2.3.9 Simulation

The above geometries were simulated in MATLAB to evaluate their length-diameter coupling.

Parameters for this study were chosen to match stents that will be used in the subsequent chapters:

Nominal stent length: 50 mm (except Hexagon 55 mm)
Nominal strut length: 5 mm
Crimped Tube Diameter: 4 mm
Crimped Tube Thickness: 0.4 mm
Strut Thickness: set to 48 struts around the stent circumference (0.262mm)
n_a,n_c set to match above parameters with maximum number of cells
Radius of Bending: 0.3 mm (from observation of manufactured stents)
Stent Strut Angle: Array from 0 to $\pi/2$, with 50 increments

The resulting length-diameter curves are reported in Figure 2.5.

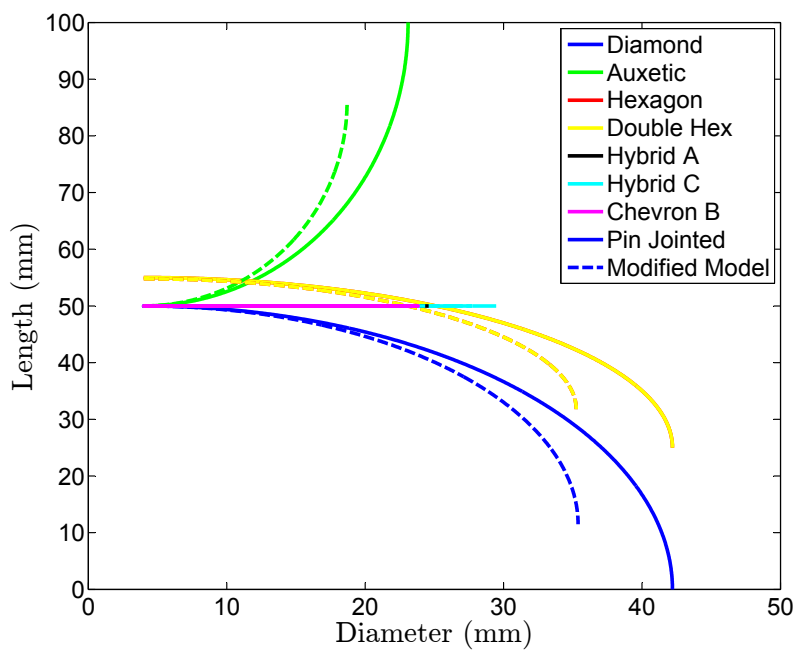

Figure 2.5: The pinned jointed model of length versus diameter.

2.3.10 Pin Jointed Analytical Discussion

The pin jointed mechanics of the stent finds that the Auxetic design has a negative effective Poisson ratio, the Hybrid A, Hybrid C, and Chevon B have near zero effective Poisson ratios, and the Diamond, Hexagon, and Double Hex designs have positive effective Poisson ratios. These results are consistent with previous FE finding from Tan et al [3]. The Chevron B is a new design also showing the interesting zero-foreshortening property. This design also has zero-foreshortening without requiring a hybrid unit cell design, instead the strut configuration is designed so local axial strains are canceled over the macro-structure.

These results also predict the maximal diameter that a given stent is able to attain. As the plots become vertically asymptotic, the struts of the stent are rotating to become almost totally in the circumferential direction. In practice, stent expansion stops before this state, especially after the recoil of the stent that occurs when the expansion balloon is deflated. The finding here is that the Diamond, Hexagon, and Double Hexagon designs have the greatest possible expansion for a fixed diameter; followed by Hybrid C; and the Hybrid A, Auxetic, and Chevron B designs have the narrowest maximum diameter, for a fixed strut length. This is because the diameter is a function of the number of cells in the circumferential direction, which the Diamond, Hexagon, and Double Hexagon designs have 12; the Hybrid C has 8; and the Hybrid A, Hybrid C, and Chevron B designs have 6. The differing number of cells in the circumferential direction is a result of the manufacturing considerations in making these cellular designs. The Diamond, Hexagon, and Double Hexagon designs are simple slotted tubes, whereas the other designs require a more intricate pattern that causes more circumferential space to be needed for a given cell.

One interesting finding is that the effective Poisson ratio is dependent on strut expansion angle as well as geometry. All stents start as slotted tubes, where the cell is similar to a square geometry, which has a zero effective Poisson ratio. As the stent opens and the stent struts rotate through an expansion angle (refer to Figure **??**), the effective Poisson ratio is highly depen-

dent on strut angle for all non-zero foreshortening designs. At the maximum stent diameter (and thus maximum strut angle), the length-diameter relation becomes a vertical asymptote for non-zero foreshortening designs (refer to the Diamond, Auxetic, Hexagon, and Double Hexagon designs in Figure 2.5). Thus, the ratio of rate of length change to rate of diameter change at the theoretical maximum diameter is infinite. In practice, stent struts to not expand to the maximum angle (90 degrees), especially when accounting for elastic recoil of the stent when the expansion balloon is deflated.

It would be possible to get the same number of circumferential cell repetitions for different cell designs by varying the strut thickness or diameter of the tube the stent is cut into. Thinner struts have been shown to have less stress induced in the artery [24], but there would presumably also be implications for the compliance and strut fracture risk of the stent. Varying the diameter of the tube the stent is cut into will cause a larger device that needs to be navigated through the body. In general, design of endovascular tools and devices is pressured to allow them to be used in smaller vessels. Thus, smaller diameter stents in the crimped (pre-expanded) state are preferred.

In addition to cell size, strut length is the other main parameter governing stent diameter. Therefore, it is possible to achieve larger or smaller maximum diameters of the stents by simply adjusting the struts to be longer or shorter, respectively. However, other performance parameters are also effected. For example, longer struts will cause the area bounded by the metal of a stent cell to be larger, allowing for greater prolapse of the artery into the stent.

When the empirically-derived correction factor for non-zero bending radii is included in the modified pin-jointed model, the predicted diameter curves are, in all cases, stretched to have a reduced predicted diameter. This effect is more pronounced at greater expansion diameters. This is because, at greater expansion diameters, the struts of the stent have rotated through greater angles. As they do this, a significant portion of the strut's length is used up in the continuous curve that is needed to keep the stent struts continuous at the nodes where multiple struts come together.

2.4 Reid-Reddy Based Analytical Model

The constant radius of curvature parameter does not account for bending plasticity in an ideal way. The empirical nature of this model requires that struts of different scales would have to be tested to give this parameter for stents of different sizes. Stent struts of different dimensions, materials, and scales would not be expected to have the same bending radius. Accordingly, a kinetic-based model is proposed that internally accounts for the bending radius that develops in the stent strut. In this section, the stent strut is simplified to a cantilever with a rectangular cross section. The bending axis has a length of the stent tube thickness, and the orthogonal axis has a length of the strut thickness at the outer diameter of the stent. The stent tube thickness is the thickness of the hollow tube the stent is originally cut from; the strut thickness is determined by how wide the slots cut into the hollow tube are decided to be.

2.4.1 Formulation

In the centre of the length of a stent strut being expanded, there is assumed no bending moment as there is an inflection point in the centre of the beam. Half of the length of one strut is then considered as a cantilever, with the loading being a point force applied at the end of the cantilever, in the direction perpendicular to the initial cantilever position. Reid and Reddy produced a model for a rigid-linearly hardening material to account for the development of plastic hinge bending zones in high-strain cantilevers [41]. An illustration is provided in Figure 2.6 to outline parameters used in the Reid-Reddy cantilever. The Reid-Reddy cantilever analysis is summarized here foe completeness.

The formulation of such a cantilever is as follows:

$$\psi_0 = asin(2p^2 - 1) \tag{2.37}$$

where ψ_0 represents the angle of the deflected, rigid portion of the cantilever

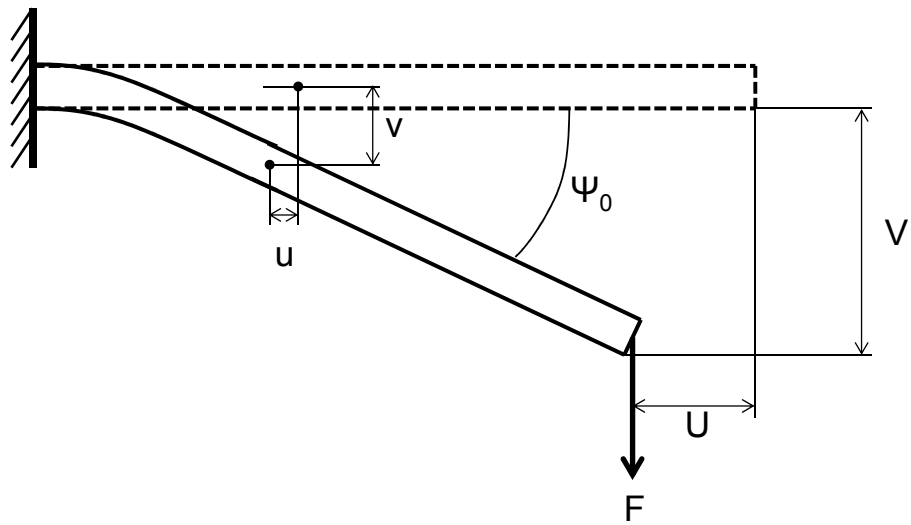

Figure 2.6: Illustration of parameters for the Reid-Reddy based method. The point u and v are measured from is the plastic-rigid transition point. The dashed cantilever is without loading, the solid cantilever is with the load F.

from the horizontal and p^2 is a parameter with values in the range between 0.5 and 1.

$$\phi_1 = asin\left(\frac{1}{\sqrt{2p^2}}\right) \tag{2.38}$$

where ϕ_1 is a parameter used in solving several incomplete elliptic integrals. Note that the p^2 is a correction of a typo in the originally published version, which had read p. The method continues with the equation:

$$b = \frac{E_p I}{M_0 \frac{L}{2}} \tag{2.39}$$

where b is a dimensionless ratio, E_p is the tangent modulus for the plastic hardening zone, L is the strut length, and length M_0 is the initial fully plastic bending moment at the cross-section where the hinge initially forms:

$$M_0 = \frac{wt^2\sigma_0}{4} \tag{2.40}$$

The load factor $\lambda = \frac{F}{F_0} = \frac{FL}{2M_0}$, is then calculated by the elliptical equation

$$\lambda - r[K(p) - F(p, \phi_1)]\lambda^{\frac{1}{2}} - \frac{1}{2p\sqrt{1-p^2}} = 0 \tag{2.41}$$

where K(p) is complete and F(p,ϕ_1) is the incomplete elliptic integral of the first kinds, and F is the point load applied to the cantilever.

A value used in computing the force-displacement relation is

$$a = \frac{L}{2} - \left(\frac{E_p I}{P}\right)^{0.5} [K(p) - F(p, \phi_1)] \tag{2.42}$$

The deflections of the point of the beam at the interface of plastic and rigid segments are then:

$$u = \frac{L}{2} - a - \left(\frac{2E_p I}{P} sin(\psi_0)\right)^{\frac{1}{2}} \tag{2.43}$$

for the foreshortening of the cantilever and

$$v = \frac{E_p I}{P}^{\frac{1}{2}} [K(p) - F(p, \phi_1) - 2E(p) + 2E(p, \phi_1)] \tag{2.44}$$

is the displacement of the cantilever, where E(p) and E(p,ϕ_1) are the com-

plete and incomplete elliptical integrals of the second kind, respectively.

Therefore, the total displacements of the cantilever are

$$U = u + a[1 - cos(\psi_0)] \tag{2.45}$$

for the total foreshortening of the cantilever and

$$V = v + asin(\psi_0) \tag{2.46}$$

is the total deflection of the cantilever.

These displacements are then applied to the cell geometry and multiplied by the number of cells in each direction to find the total displacements of the stent. Recall that each stent strut consists of two cantilevers. Thus, the diameter of all stents except the Double Hexagon is expressed as:

$$D = D_o + \frac{4n_c V}{\pi} \tag{2.47}$$

and Double Hexagon is

$$D = D_o + \frac{8n_c V}{\pi} \tag{2.48}$$

where D is the stent diameter and D_o is the pre-expansion diameter of the stent.

The length of a Diamond, Hexagon, or Double Hexagon stent can be described as

$$L = 4n_a\left(\frac{l}{2} - U\right) + L_o \tag{2.49}$$

where the factor 4 represents that there are four cantilevers axially per unit cell, and L_o represents the fixed length portion of a stent. This portion

includes the lengths of axially running struts that do not rotate with expansion, connectors linking struts together at nodes, and slots cut into the tube as required to create cell designs when considering manufacturing limitations.

Similarly, the length of an Auxetic stent is

$$L = 4n_a\left(\frac{l}{2} + U\right) + L_o \tag{2.50}$$

and the Hybrid A, Hybrid C, Chevron A, and Chevron B stents are

$$L = 4n_a\left(\frac{l}{2} + U + \frac{l}{2} - U\right) + L_o \tag{2.51}$$

which reduces to

$$L = 4n_a\left(2\frac{l}{2}\right) + L_o \tag{2.52}$$

The stent designs are then simulated in MATLAB using the same geometric parameters as the pin-jointed model. The material parameters are as follow:

$\sigma_0 = 260$ MPa [42], $E_p = 692$ MPa [43]

2.4.2 Reid-Reddy Method Results

The resulting length-diameter curves are reported in Figure 2.7. Similar to the pin-jointed model, this model predicts elongation for the Auxetic design, zero foreshortening for the Hybrid A, Hybrid C, and Chevron B designs, and foreshortening for the Diamond, Hexagon, and Double Hexagon designs. The maximum expansion diameters are also predicted as the end points of each curve. Diamond, Hexagon, and Double Hexagon all have the largest predicted maximum diameter.

Another advantage of the Reid-Reddy method is that the formulation is not purely geometrical: it does account for loading on the struts and thus

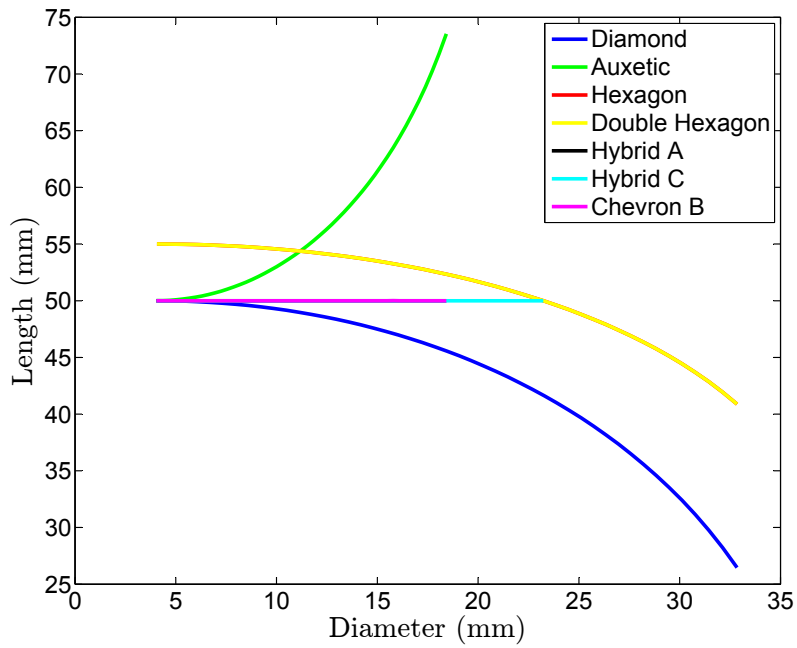

Figure 2.7: The Reid-Reddy length versus diameter relation.

the comparative stiffness of the stents during expansion should be able to be predicted.

The force-deflection relation is shown in Figure 2.8. This relation could be used to make to a pressure-diameter relation. An attempt to do this is documented in the First Appendix, with the remainder of the method being allocated to future work. There is limited clinical benefit to knowing the pressure-diameter relation precisely, the major constraint is maximum balloon pressure and force the surgeon must apply to expand the stent.

2.4.3 Reid-Reddy Analytical Discussion

The length-diameter results using the Reid-Reddy based method are similar to the results when using an empirically based correction of the pin jointed

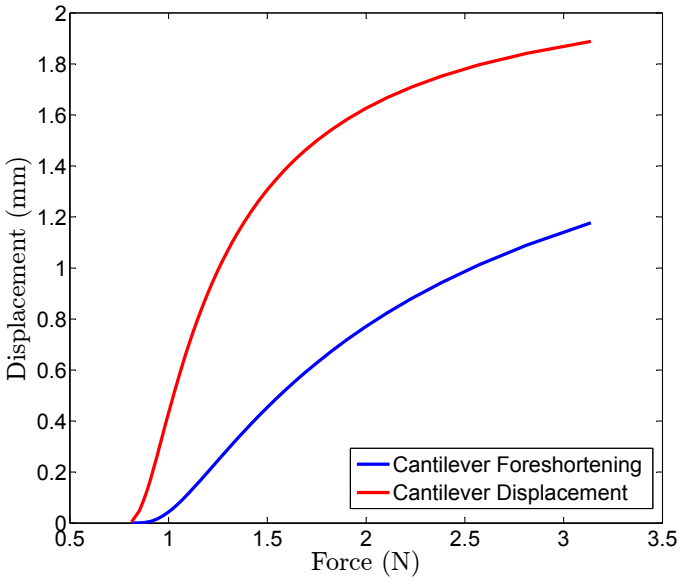

Figure 2.8: The force-displacement relations for deflection and foreshortening of a Reid-Reddy cantilever.

models. The Diamond, Hexagon, and Double Hexagon designs were all found to foreshorten as they expand. The Hybrid A, Hybrid C, and Chevron B designs do not foreshorten as they expand. The Auxetic design elongates axially as it expands.

This method also allows the prediction of a stent's maximum diameter, given parameters of its unit-cell level design. The Diamond, Hexagon, and Double Hexagon designs were again predicted to have the maximum possible diameter of the designs when controlling strut length. The Hexagon and Double Hexagon designs were predicted to have the same diameter-length relation. This suggests that non-bending, axially running struts can be removed without effecting the stent's axial strain through expansion. Removing axial struts would allow the stent to have a lower bending stiffness, potentially allowing it to be more tractable in navigating to arteries and

more able to conform to curved arteries it may be expanding into. However, removing axial struts also increases the unsupported area in the stent that the artery can prolapse into.

Also, this model assumes that a stent expands at a constant diameter along its length. In reality, the complex balloon-stent interaction expands different parts of the stent at different rates. This model could perhaps be adapted in the future to include this by assuming an expansion at a constant pressure, then calculating the expanded diameter at different struts along the stent's length.

2.5 Stent End-Condition Mechanisms

A brief finite element study was preformed to determine the influence, if any, of how stent struts connect together at nodes on the mechanics of the stent's expansion.

Due to fabrication constraints, different strut designs have different connections at nodes. The Reid-Reddy model assumes a cantilever encastered at its boundary. The "slotted tube" mechanism on the Diamond, Hexagon, and Double Hexagon stents are probably closest to this, but still allows limited rotation at the boundary. Other mechanisms of connecting the strut at the node were thought to allow even more. Cantilevers were extracted from half-strut models from the CAD models used in creating the finite element models. These cantilevers were then transfered to the finite element simulation program Abaqus CAE, and simulated using the following parameters:

Boundary conditions were applied according to symmetry conditions at the nodes, and loading as a distributed force acting on the cut surface of the stent strut. The load is applied perpendicular to the cantilever, and without surface following so the force vector remains in this direction. This load was applied as a ramp, to a maximum of $4x10^7$ N/mm^2. Given the cross-sectional area of the strut, this corresponds to a 3.77 N point load on each strut, which is comparable to the forces predicted in the Reid-Reddy analytical model (see Figure 2.8. The mesh was created with tetrahedral elements, with a global size of 0.041, curvature control of 0.025, and the minimum size factor

of 0.025. Note that the base units used were millimeters.

The material was modeled using common steel material values, with the following parameters:

Density: 7980 kg/m^3
Elastic Modulus: 200 GPa
Poisson Ratio: 0.3
Plastic Yield: 300 MPa

The FE model was solved using the iterative, Full Newton method. Displacement at representative nodes was exported for further processing in Excel and MATLAB. The Reid-Reddy yield stress was adjusted 300 MPa for this analysis.

2.5.1 Slotted Tube Hinge

The slotted tube mechanism is closest to the encastered cantilever, as there are fixed boundary conditions both vertically and horizontally relative to the cantilever, by symmetry. It is found in the inside struts of the Diamond, Hexagon, and Double Hexagon stent designs. This was predicted to be the stiffest mechanism as it is closest to the fully constrained end condition. Figure 2.9 shows the finite element results.

2.5.2 Foot-Foot Hinge

The foot-foot mechanism has a short connector laterally from the cantilever to the symmetry-based boundary location. The symmetry based boundary section extends both above and below the connector. The connector is 1.5 strut-thicknesses wide. This mechanism is found in the Hybrid C and Chevron A designs. Figure 2.10 shows the FE model of this mechanism.

2.5.3 Free-Free Hinge

The free-free mechanism (see Figure 2.11) also has a short lateral connection from the cantilever to the symmetry-based boundary location. However, the

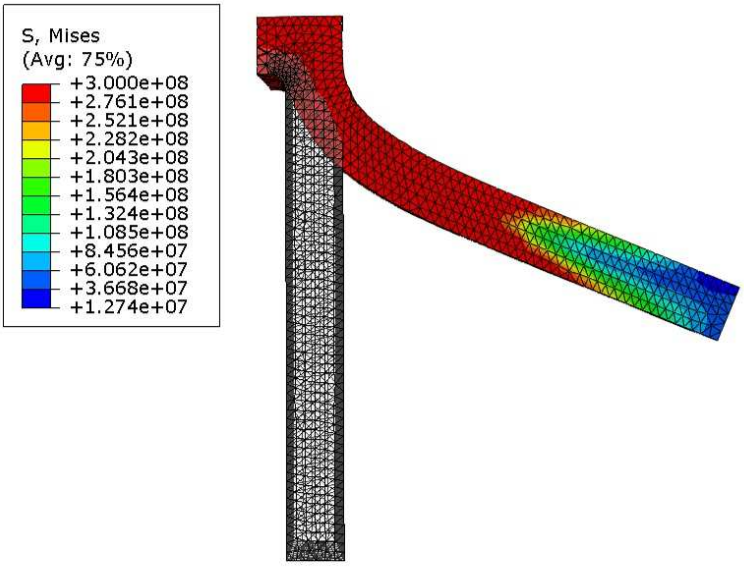

Figure 2.9: FE of the slotted tube cantilever node connection mechanism. The load is applied at the tip of the cantilever in the horizontal direction.

symmetry condition involved here results in a connector that is 0.5 strut thicknesses wide. The mechanism is found at low nodal connectivity nodes, for example the ends of a Diamond, Hexagon, or Double Hexagon stent. This was predicted to be the least stiff mechanism, as it has the least support and it could be an explanation for the dogbone effect seen at the ends of Diamond stents. The dogbone effect is a localized over-expansion of the ends of a stent that is clinically noted.

2.5.4 Free-Foot Hinge

The free-foot mechanism (see Figure 2.12 has a 1.5 strut-thick connector like the foot-foot mechanism. It differs in that the connection to the boundary surface extends from the strut connector only in the direction of the cantilever and not the opposite. It was hypothesized this mechanism may have less stiffness than the foot-foot mechanism.

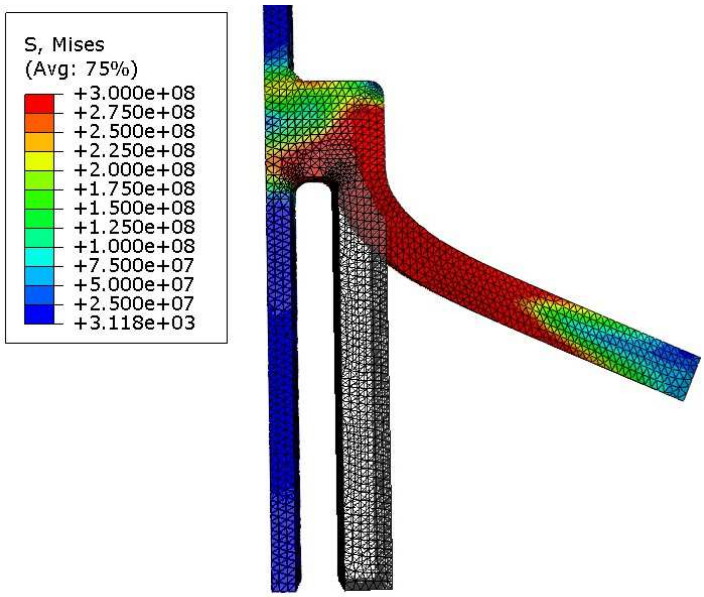

Figure 2.10: FE of the foot-foot cantilever node connection mechanism. The load is applied at the tip of the cantilever in the horizontal direction.

2.5.5 Results of FE Cantilever Study

Figure 2.13 shows the results of the finite element study, compared with theory by Reid-Reddy. The resulting plots are quite similar for each connection. Interestingly, the foot-foot mechanism was found to have the highest compliance, and the free-free mechanism has the lowest compliance. It is important to note that in addition to the actual connector mechanism, the are some variance between bending lengths of different cantilevers studied here due to manufacturing constraints in making these designs.

As all of these results are quite close to one another, no correction factor was added to the analytical results. Future work could include a factor to account for the different end mechanisms of different unit cells.

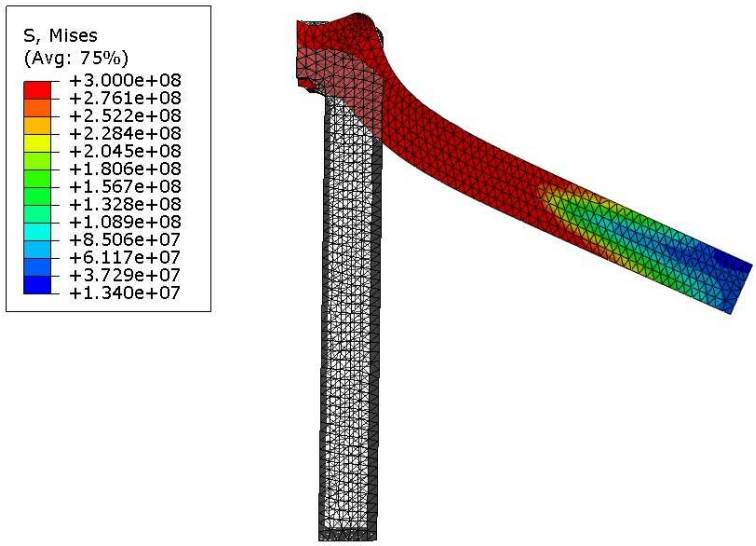

Figure 2.11: FE of the free-free cantilever node connection mechanism. The load is applied at the tip of the cantilever in the horizontal direction.

2.6 Limitations

A stent typically has a small number of cells, leading to a greater effect from end effects when describing the mechanics of the stent by lattice theory. One common end effect is the dog-bone flaring effect, often seen as a result of the balloon expansion of a stent. End effects are not included in this analysis. Bending of circumferentially-running connecting struts is not considered. This method also assumes that stent struts throughout the stent expand at the same rate. In reality, the balloon expandable stents typically expand in a way that different parts of the stent expand before others.

The constant radius of curvature parameter does not account for bending plasticity in an ideal way; its empirical nature requires that different scale stents would have to be tested to give this parameter for stents of different sizes. For example, the stents analyzed in this thesis are on the large end of stent sizing. Smaller scale stents could be expected to have a different,

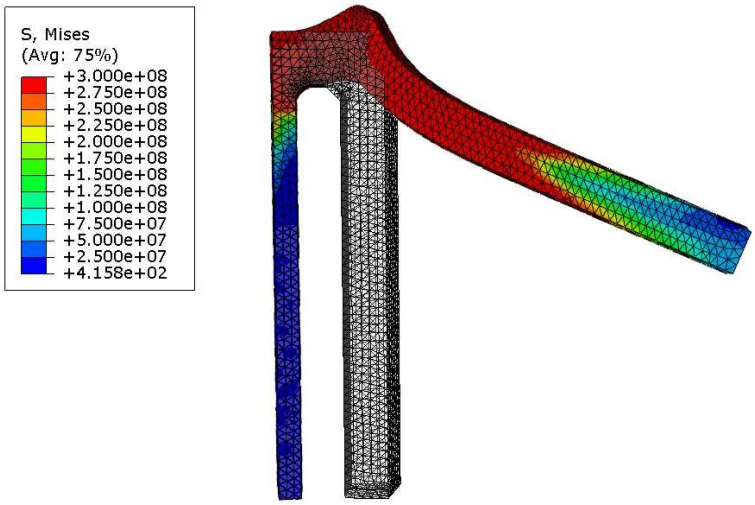

Figure 2.12: FE of the free-foot cantilever node connection mechanism. The load is applied at the tip of the cantilever in the horizontal direction.

shorter radius of curvature.

The analytical models consider loading from radially outward pressure only, and do not consider axial friction with the balloon. This could be added to the model by including an axial-displacement dependent shear force.

The geometry of the artery the stent is expanded into is assumed to be a straight, constant radius tube. True arteries requiring stents are rarely straight or having a constant radius.

The Reid-Reddy model appears to be an improvement on the pin-jointed model, but has limitations. Compliance should be able to be calculated using this model, but a confident result has yet to be achieved. The math involved is also more complicated, creating for a slightly longer simulation time and limiting the method to software that includes elliptical function solvers.

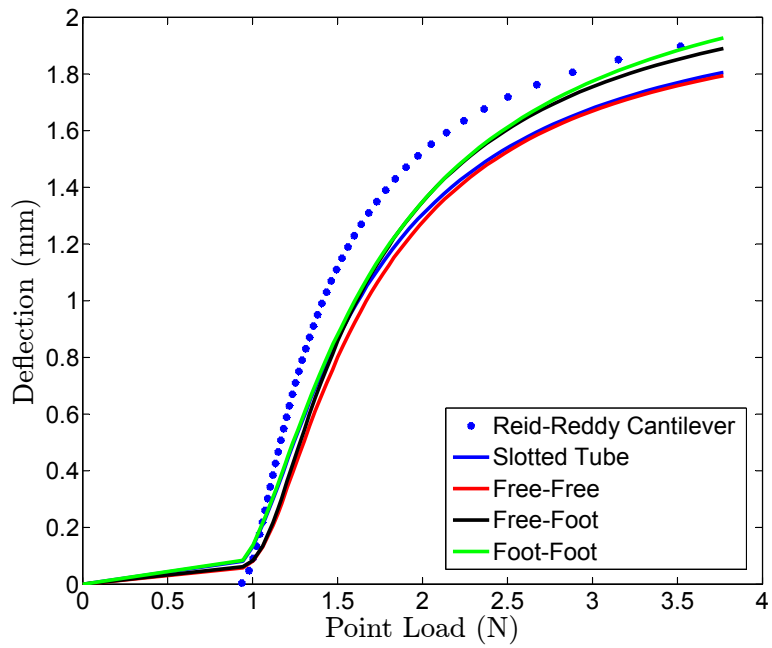

Figure 2.13: Cantilever FE simulations, along with the Reid-Reddy analytical prediction

2.7 Conclusions

Analysis of stents analytically is a promising method for rapid design calculations different stent designs quickly. The method is limited in that only geometric information is currently received from it, but early experience shows a good match to FE analysis, as will be presented in Chapter 3. Future work should focus on using this method to get solid mechanics information (such as compliance), design optimization of stents, and in further validating the model through FE and experiments.

Chapter 3

Finite Element Analysis of Stent Expansion

3.1 Introduction

Candidate stent designs are now further examined by finite element analysis (FE). FE is a common tool for the computational analysis of stents, and engineering design in general. Compared to analytical methods, it has the advantage of providing stress distributions within the stent; it is possible to model contact with other structures such as the balloon and artery; and the model can account for elastic, plastic, and other properties of the stent. A drawback, however, is that stent designs take considerably longer to model, simulate, and change than analysis through analytical methods presented in the previous chapter.

Candidate stent designs are first modeled in a CAD program. The CAD model is then imported to Abaqus CAE, where the stent is given a mesh, material properties, boundary conditions, and a pressure loading condition. The FE simulation is run in Abaqus Standard. From the simulation, pressure and nodal displacement data is exported, then converted to a text and then an Excel file. Excel is used to convert nodal displacements to stent diameter. The data is then imported to MATLAB for graphing the results.

Two stages of FE are conducted for the same stent CAD models. The first stage is expansion with a common pressure (1 MPa). The second stage is expansion to a common target diameter (18 mm).

3.2 Modeling of Candidate Stent Designs

Additional FE is preformed on the Diamond, Auxetic, Hybrid A, Hybrid C, and Chevron B designs.

The Double Hexagon design is dropped from consideration as it will result in only three struts supporting the stent axially at each axial cell repetition. This would encourage prolapse of the artery into the stent, and lacks redundancy in the case of stent fracture. The Hexagon design is also removed from consideration as it is simply a Diamond design with the node connectors linking cells axially elongated to one strut length. The Chevron A design, being essentially a Hybrid C design with alternate strut pairs switched in orientation, is also removed from consideration given its similarity to the Hybrid C design.

The remaining five candidate designs are modeled in NX 6.0 (Seimens) in preparation for FE and manufacture. The design starts from 50 mm long hollow tubes, with a 4.0 mm outer diameter and 0.40 mm wall thickness. The cross section was chosen due to this size being available as stock from Lumenous Device Technologies, who manufactured the stent designs for this study.

Strut lengths were modeled after the approximate dimensions of a large diameter sample Palmaz-Schatz stent, with the nominal strut lengths being 5 mm. Thus, there are 10 strut lengths per stent. In the circumference, the Palmaz Schatz sample stent has eleven cells. As each Diamond cell requires four strut thicknesses, it was decided to increase the number of cells in the circumference of the Diamond stent to twelve, such that the circumference of the stent would be 48 strut-thicknesses. This allows the circumference to be easily divided into cells requiring a different number of strut-thicknesses: 4 (Diamond, Hexagon), 6 (Hybrid C, Chevron A), 8 (Auxetic, Double Hexagon, Hybrid A, Chevron B), and 12 (more open versions of these designs). Therefore, the strut thickness is the outer circumference divided by 48.

Slots are made into the tube by sketching sectors on the cross-section of the tube, and using the $extrude - subtract$ function to remove material

from the part model. All slots passing into the stent have their side edges filleted with a radii of 0.08 mm.

3.3 Methods

3.3.1 Simulation Strategy

Two stages of FE simulation are preformed. For the first, all stents are loaded with the same 1 MPa pressure applied to the inner surface of the stent. This step is used to compute the length-diameter relation and compliance of the stent to the maximum diameter. Then, the pressure required for each stent to expand to a common target diameter of 18mm is calculated from this data, and the simulation is re-run using design specific pressures to reach the target diameter. This allows the recoil, compliance, and foreshortening to be compared across designs for the same nominal vessel size.

3.3.2 Model Parameters

The five candidate designs are imported to Abaqus CAE 6.8-4 as .IGES files. The models are taken as one-eighth sections of the full stent, using two planes of radial symmetry to reduce the size of the problem, and one plane of axial symmetry or assumed congruency. The Diamond, Auxectic, and Hybrid C designs have axial symmetry. The Hybrid A and Chevron B designs, by nature of their construction, do not have axial symmetry but are assumed to have repeated mechanics due to the periodicity of the structure. With a different length and/or construction, the Hybrid A stent could have axial symmetry; the Chevron B can never have axial symmetry, although the two halves of a sliced stent are the same with a one-half cell rotation about the axis of one of the stents.

The planes are intentionally selected to pass through the mid-plane of nodes where stent struts intersect. The radial planes of symmetry are also selected to lie on the XY- and XZ-planes of the Cartesian coordinate system, or a new coordinate system is created to satisfy this condition. The X-axis here represents the line defining the center of the stent.

A fine mesh is required as the stent has a highly non-linear geometry changes as well as non-linear material properties. Simulations use on the order of 300 000 elements when meshed according to the parameters below.

Mesh qualities are somewhat quantized due to the slender nature of the struts. Typically, there are four or five elements across the strut width. Thus, to increase the mesh quality to having six elements across a strut width, the total number of elements in the model must increase by 1.2^3, or 73%. It is easier to increase mesh size in the nodes of the stents without having such a penalty in increasing the size of the problem, but their contribution to the strains seen in stent expansion is limited.

All simulations used the following mesh parameters:

Element Type: C3D4 (a 4-node, 3D stress tetrahedral element)
Maximum Deviation Control (for curvature): 0.08
Minimum Size Factor: 0.05

Additionally, Table 3.1 gives approximate global sizes were applied to mesh the stents:

	Diamond	Auxetic	HybridA	HybridC	ChevronB
1 MPa Ramp	0.0574	0.06	0.0625	0.0625	0.06
18 mm Diameter	0.065	0.072	0.0675	0.0625	0.0625

Table 3.1: Mesh Parameters for Approximate Global Size.

The parameters in the above table were found iteratively. For more coarse meshes, the step length used in the iterative solver, described in a subsequent section, becomes very small and the simulation cannot be completed. One hypothesis is that some elements exceed strain limits at some point in the simulation, and the simulation fails. Interestingly, there are times that a more coarse mesh will run to completion and a finer mesh will not run. This suggests it is individual elements rather than the mesh in general that is causing problems. Additionally, the simulation fails due to a memory error if too many elements are used in a simulation.

The material considered for the expansion is 316L stainless steel in the annealed condition. This is a common material for balloon expandable stents, and is approved for implantation. All stents had the following parameters:

Density: 8000 kg/m^3
Elastic Modulus: 193 GPa [42]
Poisson Ratio: 0.3
Plastic Yield: 260 MPa [42]

The material model is elastic-perfectly plastic. This means it has a linear modulus until yielding, then the modulus is zero. The structure retains stiffness due to geometry changes and the propagation of the plastic zone through the stent strut.

There are several models in Abaqus that account for material non-linearity. The plastic model was chosen as it will hold plastic strains, with some unloading recoil. Some other non-linear material models will recoil to the initial state when the load is removed.

3.3.3 Boundary Conditions

The boundary conditions are selected according to to the section cuts made in the stent to give it the one eighth section of the part. The boundary condition applied to prohibit motion of the section cuts out of the section cut plane. This is why it was important to select nodes located on the planes of the coordinate system of the part or to make a new coordinate system, so that the boundary conditions at each plane could be specified as ux=0, uy=0, or uz=0, respectively. A cylindrical rather than Cartesian coordinate system could be used instead, but that method still requires the creation of a new coordinate system.

3.3.4 Loading

There are two stages of simulation with two loading criteria. In the first, all stents are expanded by a 1 MPa pressure. For the second simulation, all stents are loaded with a pressure that is expected to expand the stent to 18 mm. Thus, the final pressure in the second simulation is different for all stents.

Expansion by a Common Pressure

Loading is applied as a Static, General load to the inner surface of the stent. The load is applied as a ramp to 1 MPa. The step used to simulate this loading has non-linear geometric controls (*Nlgeom*) to reduce the effect of the large, non-linear geometry changes present in the simulation. The step has automatic incrementation to a maximum of 200 increments, with a minimum increment size of 1E-5 of a step size of 1. The step is solved using an iterative solver, using the Full Newton method, with linear extrapolation of the previous state at the start of each increment. The load varies such that it ramps linearly over the step.

Nodal displacement data is then extracted from the radial boundary condition planes and the axial end that does not have a boundary condition. This data is used to produce a length-diameter relation for each of the stent designs. The diameter data is combined with pressure data to create a pressure-diameter relation for each stent design. Finally, a compliance-diameter relation is reported for each stent design, where compliance, C is

$$C = \frac{D_2 - D_1}{D_1(P_2 - P_1)} \tag{3.1}$$

where D_1 is the diameter at one step of the output of the FE simulation, D_2 is the diameter at the next output step, P_1 is the pressure at the first output step, and P_2 is the pressure output at the second output step.

Expansion to a Common Nominal Diameter

To examine post-deployed mechanics of stents, the five stents are expanded to a common target diameter to compare their post-expansion recoil, and their foreshortening and compliance under blood pressure loading.

Excessive recoil is poor for stent performance as it will result in a reduction of lumen compared to a stent that holds its diameter once the expansion balloon is removed.

To reduce stress imposed on the artery, compliance and foreshortening should match the artery or at least should minimize stress concentrations. There are mechanobiology-based theories that suggest that stress imposed by the stent on the artery results in activating pathways promoting growth and remodeling of the artery [23]. This could cause in stent restenosis, and a reduction in lumen after stenting. This is more of a concern in narrower arteries than the aorta, but use of non-dimensionalized parameters should allow extrapolation to stents of any size.

In general, lower compliances are preferred so long as they still resist recoil of the artery. Similarly, zero foreshortening or slight elongation as the blood pressure on the stent rises from diastolic to systolic is preferred to match the artery.

18 mm was selected as a target diameter as it was an integer diameter that was near the maximum diameter of some of the stents. The pressure-diameter data for each stent was linearly interpolated to predict a pressure that would result in a post-expansion diameter of 18 mm. This pressure was then applied to the inner surface of each stent.

Two subsequent loading steps were created in Abaqus. After the balloon expansion step, a "diastolic" pressure load was created to a pressure of 10.7 kPa (corresponding to approximately 80 mmHg) as a ramp from the balloon expansion pressure. A final step used a "systolic" pressure of 16.0 kPa (corresponding to approximately 120 mmHg) as a ramp from the "diastolic" pressure.

Recoil, R is calculated as

$$R = \frac{D_m - D_d}{D_m} \tag{3.2}$$

where D_m is the diameter at the end of the balloon expansion step, and D_d is the diameter at the diastolic pressure, after the stent has recoiled.

Foreshortening, f is calculated as

$$f = \frac{L_s - L_d}{L_d} 100\% \tag{3.3}$$

where L_d is the length of the stent at diastolic pressure and L_s is the length of the stent at the systolic pressure.

Material properties are the same as the 1 MPa step. Mesh parameters change as according to Table 3.1.

3.4 Results

3.4.1 Maximum Expansion Length-Diameter

The results of the finite element study on the Diamond, Auxetic, Hybrid A, Hybrid C, and Chevron B stent designs are in shown Figure 3.1. The Diamond design again shows significant foreshortening, while the Auxetic design has axial lengthening with expansion. The Hybrid C design has no foreshortening. Interestingly, the Hybrid A and Chevron B have small negative effective Poisson ratio. Both were predicted to have a near-zero effective Poisson ratio due to these designs having zero foreshortening using the analytical method in Chapter 2.

The resulting pressure-diameter relation for the five stents tested using FE is shown in 3.2. The Diamond design is seen to have the largest expected diameter, followed by the Hybrid C, and finally the Auxetic, Hybrid A, and Chevron B designs have the narrowest diameter.

All stents yield at similar points, at around 200 kPa of pressure, although the Auxetic and Hybrid C designs appear to yield slightly earlier and the

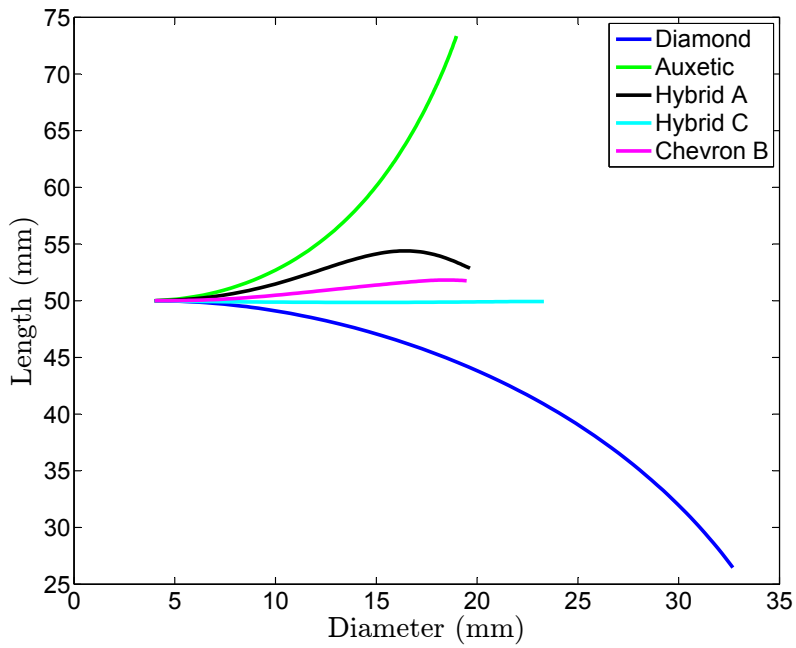

Figure 3.1: FE simulation for length versus diameter.

Hybrid A design yields slightly later than the Diamond and Chevron B designs. All designs have a similar linear zone until about 200 kPa of pressure. After yielding, the graphs of stent expansions show different curved plastic regions for each design. These curves become more horizontal as the stent approaches its maximum diameter. Portions of the curve that are more horizontal are when the stent expansion is stiffer, or less compliant.

Note that the linear elastic phase before yield at around 200 kPa results in very little diametric strain, with the stent becoming plastic with less than one millimeter of diametric expansion. This supports the use of a plastic hinge assumption used in the analytical section of this thesis as the elastic phase of stent expansion contributes little to the full expansion of the stent.

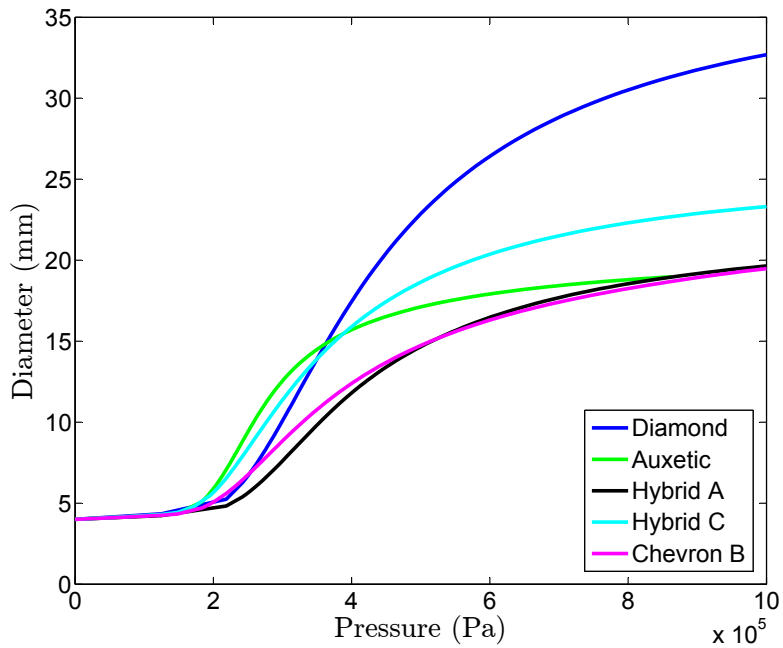

Figure 3.2: FE simulation for pressure versus diameter.

3.4.2 Maximum Expansion Compliance-Diameter

The compliance versus diameter relation for the stents is shown in Figure 3.3. Higher values of compliance indicate that the stent experiences relatively more strain for a given pressure. All stent designs have the same general pattern of compliance against diameter. There is a rapid rise in compliance until the yielding phase, then compliance peaks. As the diameter expands, the compliance decreases. The phase of increasing compliance appears to be similar for all designs. However, the peak compliance and the rate of compliance decrease with diameter increase depends on design.

The Auxetic design hast the highest peak compliance, but the compliance quickly diminishes as the stent expands towards its maximum diameter. The Diamond design has the second highest compliance peak, with the

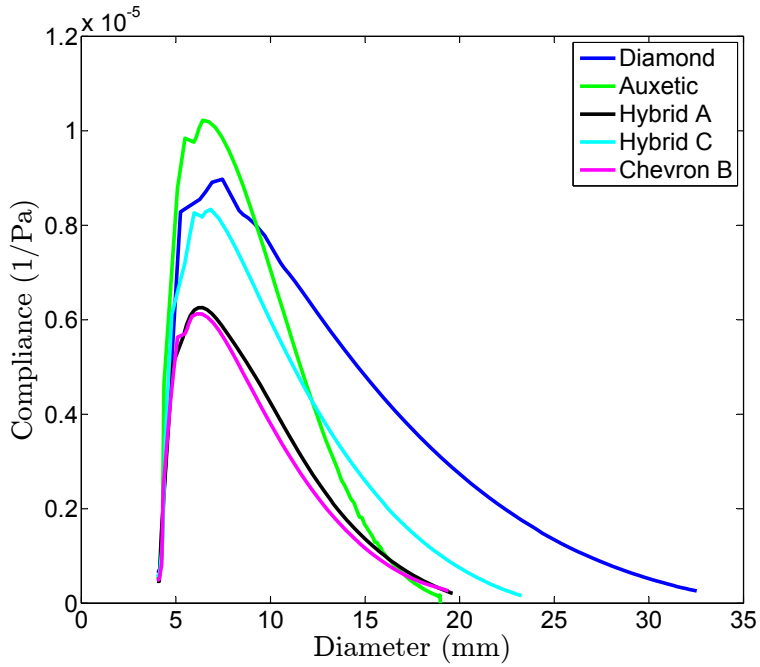

Figure 3.3: FE simulation for compliance versus diameter.

most gradual decrease in compliance with diameter. The Hybrid C design has the third highest peak compliance, with an intermediate rate of compliance decrease with diameter. Hybrid A and Chevron B have similar peak compliances and a similar rate of compliance decrease with diameter.

3.4.3 Target Diameter Recoil

The length-diameter relations for the five stents start the same as the 1 MPa simulation, until they reach the nominal target diameter and recoil as shown in Figure 3.4. The recoil for the Diamond, Hybrid C, and Auxetic designs follows the expansion curves. Interestingly, the recoil for the Hybrid A and Chevron B designs do not trace the expansion curve. Instead, they follow curves that reduce their final foreshortening.

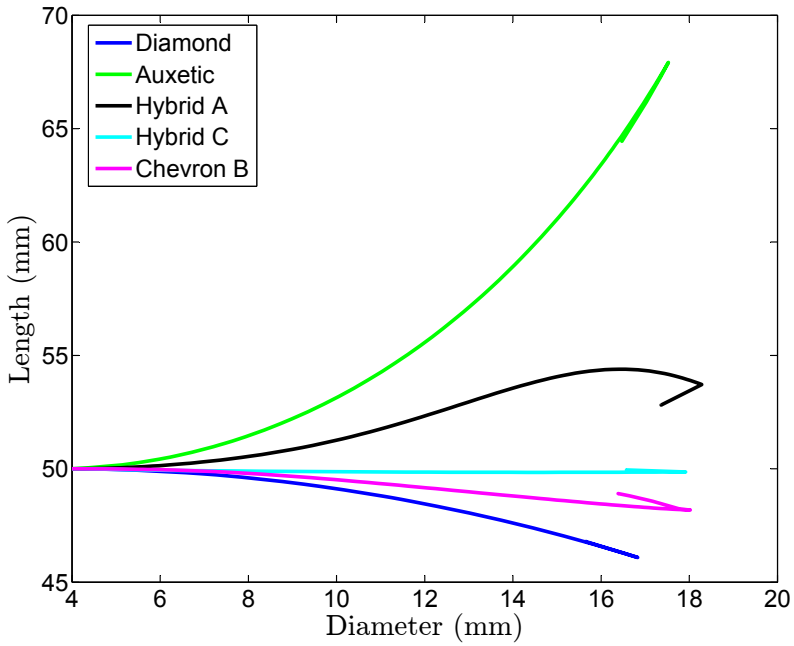

Figure 3.4: FE simulation for length versus diameter for stents expanded to approximately 18 mm then allowed to recoil.

The pressure-diameter relations for the five stents also follows the 1 MPa figure, until the balloon pressure is removed and the stents rapidly recoil (see Figure 3.5). The recoil is approximately linear and at a similar slope to the linear expansion phase before yielding.

The Chevron B stent recoiled 1.6 mm, followed by the Hybrid C (1.3 mm), Diamond (1.2 mm), Auxetic (1.1 mm), and Hybrid A (0.9 mm), as shown in Figure 3.6. The same order is preserved when the results are non-dimensionalized to diameter, shown in Figure 3.7.

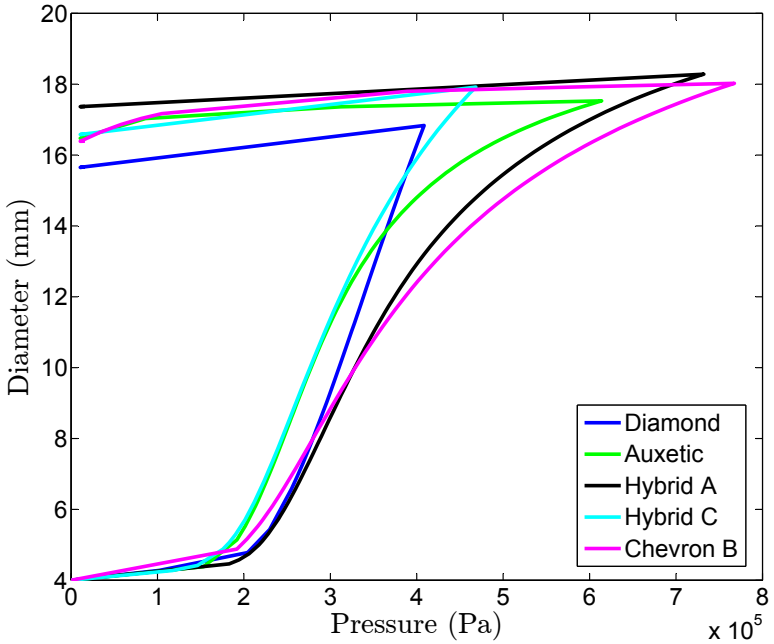

Figure 3.5: FE simulation for pressure versus diameter for stents expanded to approximately 18 mm then allowed to recoil.

3.4.4 Target Diameter Foreshortening

The foreshortening of the stents under physiologic loading is shown in Figure 3.8. The Diamond stent foreshortens by 0.015%; the Hybrid C stent has negligible foreshortening; and the Auxetic, Hybrid A, and Chevron B design elongate by 0.019%, 0.004%, and 0.002%, respectively.

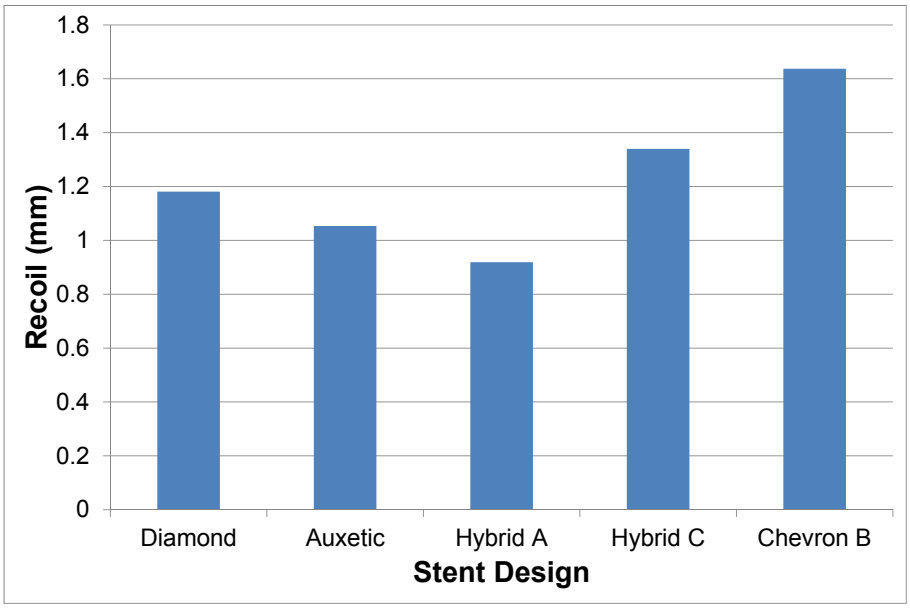

Figure 3.6: FE simulation for the recoil of the stents expanded to approximately 18 mm then allowed to recoil in millimeters.

3.4.5 Target Diameter Compliance

The highest compliance was found for the Diamond (0.15 MPa^{-1}) design, followed by the Hybrid C design (0.082 MPa^{-1}) (see Figure 3.9. The other three stents had similar compliance values: the Chevron B stent was 0.054 MPa^{-1}, the Auxetic was 0.047 MPa^{-1}, and the Hybrid A was 0.043 MPa^{-1}.

3.4.6 Observations of Stent Stress Distribution

Figures 3.10, 3.11, 3.12, 3.13, and 3.14 show the expanded FE models for the five tested stent designs. The red areas are those that have reached the plastic yield point of 260 MPa. These figures highlight that bending strain is localized to being near the strut nodes, a key assumption of the

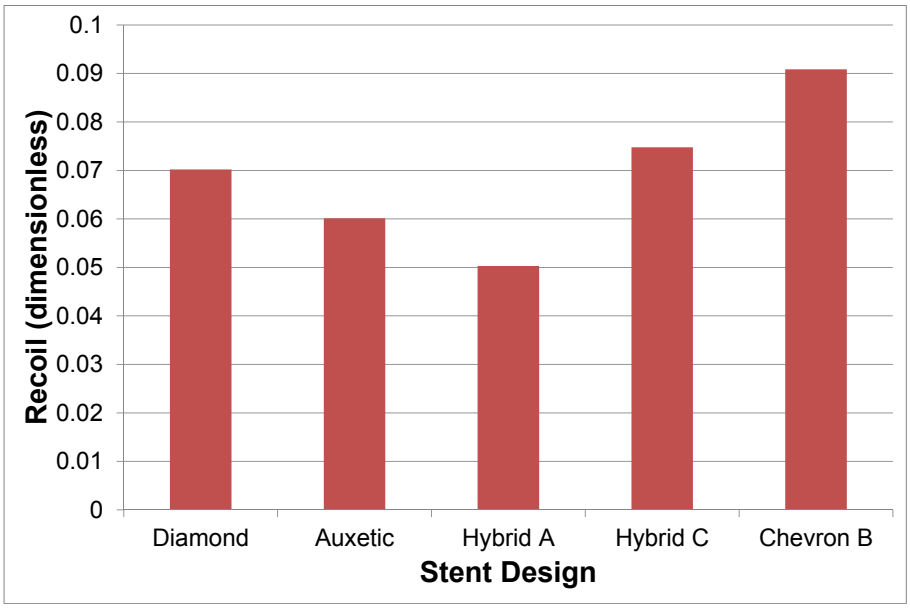

Figure 3.7: Non-dimensional results from the FE simulation for stents expanded to approximately 18 mm then allowed to recoil.

analytical model, although the yielded area does propagate beyond the zone where substantial curvature is present in the stent. Nodes of the struts are fully plastic but do not appear to contribute to the diametric or axial strain. Axial connecting struts that do not bend have lower stress, below the yield point. This was a key assumption of the analytical model, that axial connecting struts do not undergo bending and do not contribute to the axial or diametric strain of the stent.

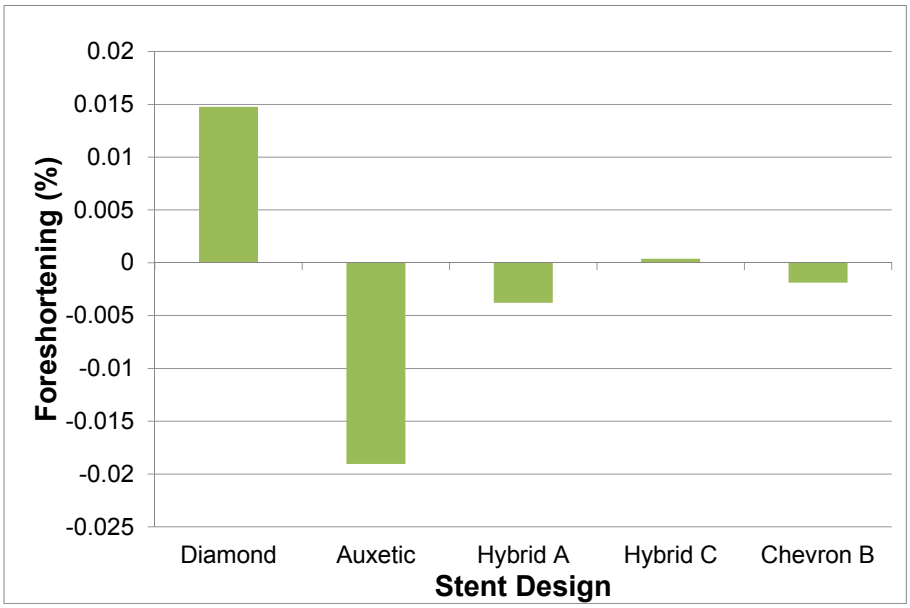

Figure 3.8: Non-dimensional results from the FE simulation for the foreshortening of the recoiled stents after systolic blood pressure is applied.

3.5 Discussion

3.5.1 FE Simulations to 1 MPa

Finite element analysis is a valuable tool in aiding stent design due to the information about stiffnesses and stresses it provides, as well as a shorter design iteration timeline than physical prototypes.

The predicted length-diameter relation for the five tested stent designs matches theory quite well. The Auxetic design elongates as it expands in its diameter, which is expected. Likewise, the Diamond design foreshortens as it expands. The Hybrid C design had a constant, zero-foreshortening expansion.

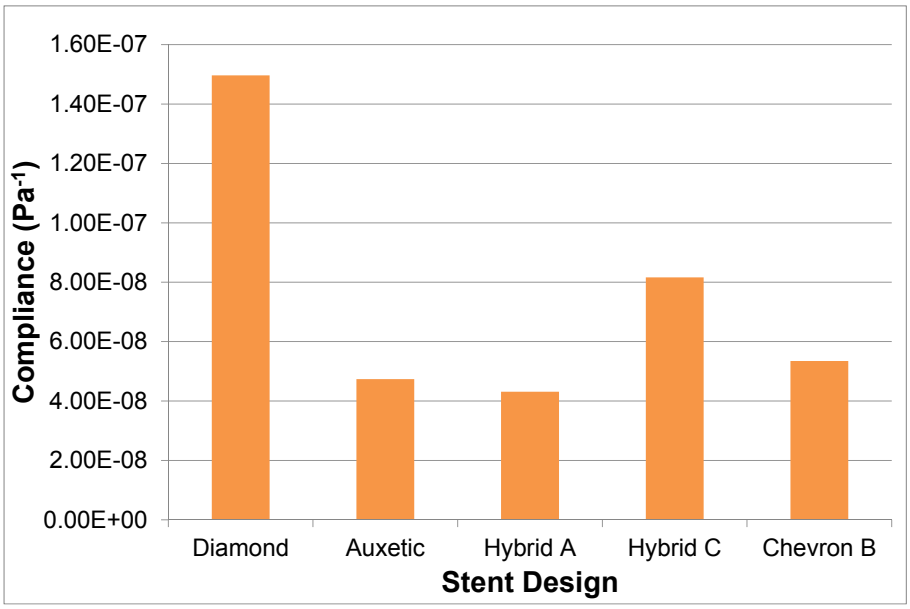

Figure 3.9: Non-dimensional results from the FE simulation for the compliance of the recoiled stents after systolic blood pressure is applied.

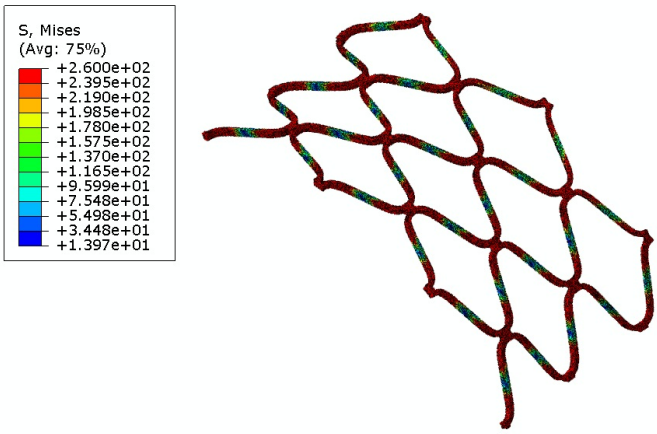

Figure 3.10: The expanded Diamond stent FE model.

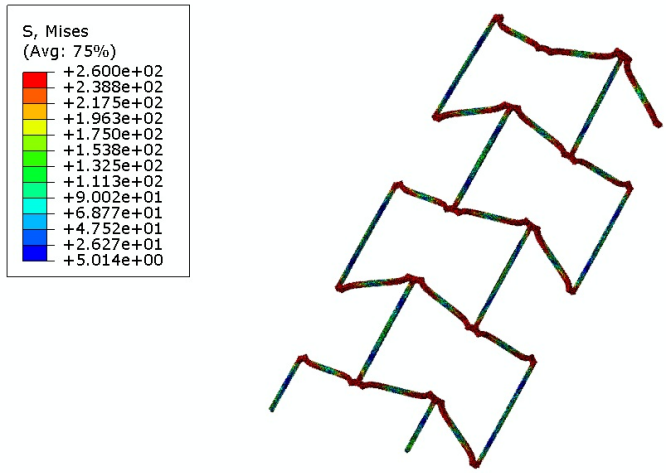

Figure 3.11: The expanded Auxetic stent FE model.

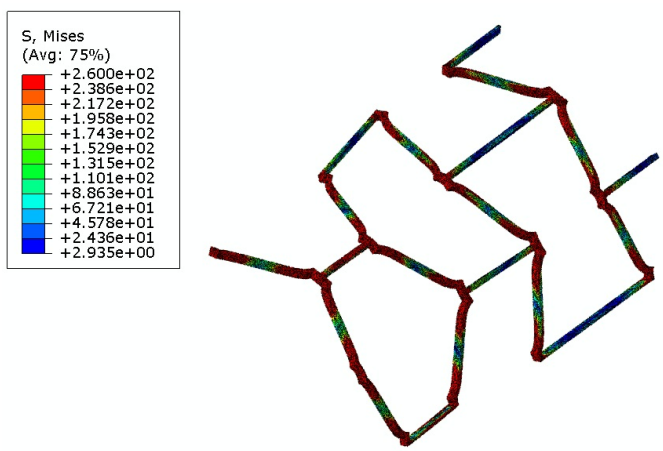

Figure 3.12: The expanded Hybrid A stent FE model.

The Hybrid A and Chevron B expansions were more interesting. The Hybrid A design elongates initially, then at about 16 mm diameter it starts to foreshorten but retains a net elongation at its final diameter. The Chevron B design initially foreshortens but at a slow rate and looks to stop foreshortening altogether.

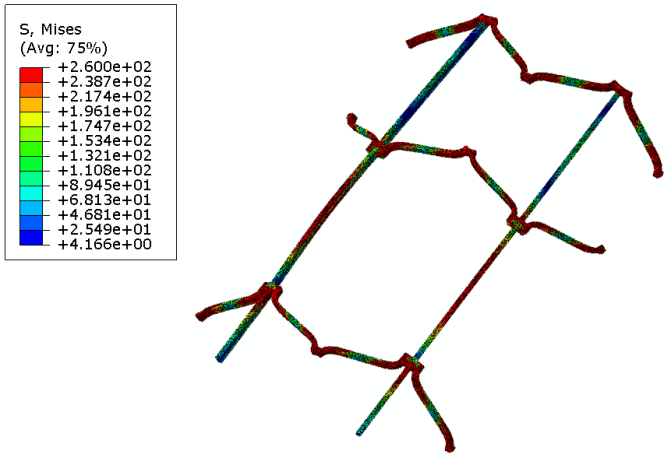

Figure 3.13: The expanded Hybrid C stent FE model.

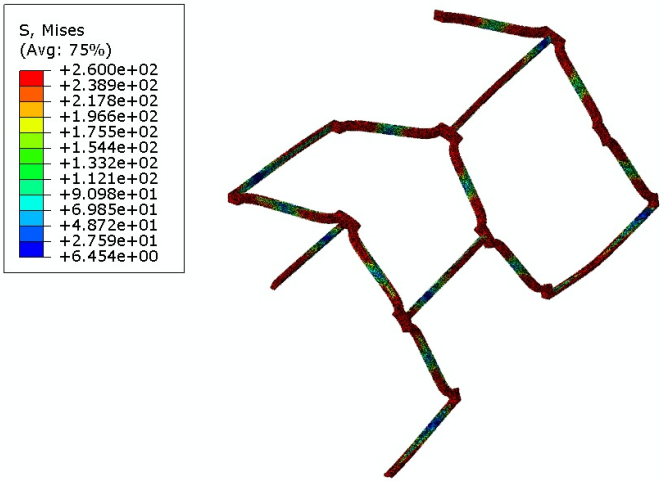

Figure 3.14: The expanded Chevron B stent FE model.

In the time history of the expansion, especially for the Hybrid A design, it is seen that different parts of the stent expand at different rates. Hybrid design have features with *local* effective Poisson ratios, but the intention is these features are arranged such that these *local* axial strains cancel each other out. It appears that since different features are expanding at different

rates, the global effect is not canceled as anticipated. For the Hybrid A design, recall the unit cell consists of a negative effective Poisson ratio auxetic cell and a positive effective Poisson ratio hexagon cell. It appears that in the simulation, the auxetic component expands faster and more than the hexagon component, giving a net elongation.

Its not clear if this phenomenon is translated to the physical world. In the FE simulation, loading is provided by an equal pressure applied across the inner surface of the stent. In real stenting, loading is provided by contact with an expanding balloon. While the balloon has a constant pressure within it, it can fold, so loading on the stent may not be spatially even. This said, stents expanded by a balloon are often seen to have non-constant rates of expansion within the stent, especially when the stent first yields. Often, the ends yield before the center of the stent due to the expansion fluid filling portions of the balloon that are not constrained by the stent first.

The maximum diameter a stent design can expand to can be seen in all graphs, but it probably best illustrated by Figure 3.2, which shows the pressure-diameter relation of the stent expansion. Here, the maximum diameter corresponds to the peak point vertically the stent expands to. This maximum diameter appears to correspond to the number of bending struts in the design: the Diamond stent has 24, the Hybrid C has 16, and the other three designs have 12. The difference in number depends on manufacturing constraints - slots cut into the original tube to make the cellular pattern have different efficiency depending on cell design choice. As noted in the Analytical chapter, larger diameters for a given design are possible by increasing strut length.

The pressure-diameter relation also shows the interesting property of the dependence of stent diameter (and therefore stent strut angle) on compliance. As the stent expands, the struts move as a plastic hinge. As the hinges rotate, the loading vector on the strut becomes increasingly more aligned with the vector direction of the strut. Thus, loading becomes less in bending and more in tension, resulting in a stiffer structure.

For compliance of the stent, the number of bending struts in the stent's circumference appears to be the most important parameter, largely for its

impact on the strut expansion angle. All stents yield at a similar point, and have similar compliances until about 15 mm diameter. Then, the stent with fewer bending struts rapidly lose compliance. Further, the three stents with only 12 bending struts (the Auxetic, Hybrid A, and Chevron B designs) have slightly different paths but end up with the same final diameter at about the same pressure.

This feature is also seen in the compliance-diameter relation figure, where compliance drops in a exponential decay-like function with increasing diameter after the peak compliance.

In both the pressure-diameter and compliance-diameter figures, the initial elastic phase of expansion is interesting. In both graphs, this phase is short, with a rapid rise in pressure or compliance with limited change in diameter. This provides justification for considering only the plastic phase of stent expansion for first-order models of stent design, as was done in the analytical section.

Pressure and compliance during expansion are probably design parameters that should be considered secondary to axial strain and target final diameter. Balloon pressure is typically not a limiting factor on stenting, as screw-assisted devices exist to increase pressure over 20 ATM (approx. 2 MPa). However, the larger diameter balloons used in the experiments to be reported later in this thesis had a rated burst pressure at 7ATM (approx. 700 kPa, for a 20 mm diameter balloon) and 4 ATM (approx. 400 kPa, for a 25 mm diameter balloon). Thus, for larger diameter balloons, stent compliance may be an important parameter to avoid balloon rupture.

However, compliance at the final diameter is highly important, and this parameter governs if the artery will collapse the stent, stress imposed on the artery by the stent, and amount of friction forces that will resist stent migration. Combined, the indication is that stent strut angle at final expansion is the design parameter to be optimized for stent performance. The parameter is influenced by target (artery) diameter, strut length, and stent cell choice.

3.5.2 FE Simulations to a Target Diameter

The Hybrid A and Chevron B designs' length-diameter relation for recoil did not follow the relation for expansion. It appears that the negative effective Poisson ratio portion of the cell causing the stent to elongate from expanding faster than the positive effective Poisson ratio portion also recoils more. This may be evidence of a further interesting property of hybrid cells: in addition to having low effective Poisson ratios and possibly having areas of different local compliance during expansion, the local recoil may change spatially through a hybrid stent design. Further study of this phenomenon is required using a contact FE model or through experiments.

The stents in the 18 mm target diameter did not all finish expansion at 18 mm. The Diamond cell was least accurate, expanding only to 16.8 mm. This discrepancy is interesting, in both simulation methods the load was applied as a linear ramp. The only parameter changed was the mesh on all stent except the Hybrid C design, which was the second closest to the target at 17.9 mm.

18 mm was chosen since it was close to the maximum diameter possible for the Auxetic, Hybrid A, and Chevron B designs. The Chevron B simulation was quite close to the target (18.0 mm), but the Auxetic (17.5 mm) and Hybrid A (18.3 mm) were further from the target than the Hybrid C design. To compensate for variability in actual diameter, the Recoil, Compliance, and Foreshortening parameters are reported as non-dimensional values. If greater accuracy is needed, one approach to try would be to do several iterations on the target pressure to attempt to and find a peak balloon expansion pressure that resulted in a diameter closer to the target diameter.

The target diameter section highlights the difficulty of multi-parameter design as is needed for stents. In this simulation, the strut expansion angle is increased to get the same diameter between stents, and the stents have a fixed nominal strut length. Alternatively, the design constraint could have been to use different strut lengths expanded to the same angle to get the same maximum diameter before recoil.

Further, the stent unit cells could have their design altered such that

there are the same number of cells repeated circumferentially. Then, the stents could have the same nominal strut length, and expand to the same diameter with the same strut rotation angle. While this approach would give more control between the designs, it handicaps stents that have more compact unit cells, allowing them to be more efficient in expansion. The recommended design process for selecting diameter is to select a unit cell design with preferred properties, then iterate on the strut lengths. Strut thickness and initial tube diameter also play a role in the final diameter of the stent.

The stent-artery interaction is neglected here. Very small strains are seen under blood pressure loading. However, blood pressure acting on the artery may cause greater stent strains through changes in the contact pressure on the stent. In these results, the foreshortening in the worst cases (Diamond and Auxetic) was on the order of 10 microns, about one animal cell size. The clinical relevance of such small strains is debatable, but strains relative to the artery may be larger if artery contact is considered.

There was a considerable difference in amount of recoil between stent designs. A low recoil is desired. The Hybrid A had the lowest recoil, and the Chevron B design had the highest. The ranked order of the stents is interesting as it does not seem to match orders seen for other performance parameters. Hybrid A and Chevron B often have similar mechanics in other performance parameters, and there is no apparent design difference that would account for them having such different recoil.

The foreshortening follows the results for the expansion FE: the Diamond design foreshortened, the Hybrid C design had a constant length, and the Auxetic design elongated. The Hybrid A and Chevron B designs also slightly elongated. Combined with the finding that recoil caused the Hybrid A and Chevron B designs to trend towards being zero-foreshortening, this result further suggests that the global mechanics of the stent are being influenced by different rates of local expansion in the stent. In lattice theory, cell repetition is often assumed to be infinite. For stents, this is often not the case: in some of the models used here as few as one cell is tested, for example in the Hybrid A design. Thus, lattice theory may be used as an in initial

guide for stent design, but refinement by considering the stent as a finite structure is subsequently required to accurately predict mechanics.

The Diamond design was most compliant, followed by the Hybrid C, and finally the Chevron B, Auxetic, and Hybrid A designs had about the same compliance. This matches the order of compliance for 18 mm for the stents while they are being plasticly expanded. With additional testing to validate this at different diameters, this would be a useful property as relative post-expansion compliance could be estimated by compliance during expansion. Recall that compliance during expansion is a less important parameter than post-expansion compliance, but compliance can be quickly estimated by the analytical model. Also recall that the ranked order of stents for compliance during expansion changed with diameter. If the ranked order also changes for post-expansion compliance, it would suggest that geometry *configuration* is important as well as cell geometry itself.

3.5.3 Comparing the FE and the Analytical Models

The length-diameter relation for the Reid-Reddy analytical and finite element approaches are reproduced for comparison (see Figure 3.15).

The length-diameter relations for both match well, in general. For Auxetic, both methods result in an expected maximum diameter of about 18 mm, a final length of about 73 mm, and a similar expansion curve. For Diamond, both methods predict a final diameter of about 33 mm, a final length of about 27 mm, and a similar expansion curve. Hybrid C is likewise similar with zero foreshortening and a final diameter of 23 mm. Hybrid A and Chevron B do not match, and deviate from the idealized zero-foreshortening model that was expected for their expansion in the finite element model.

3.5.4 Comparison of Post-Expansion Mechanics

Tan et al previously performed FE analysis on unit cell-based designs, with some overlap to the designs used in the current study [3]. The Diamond, Auxetic, Hybrid A, and Hybrid C designs are used in both studies. The stents in the Tan study were of a 3 mm nominal diameter, and were loaded

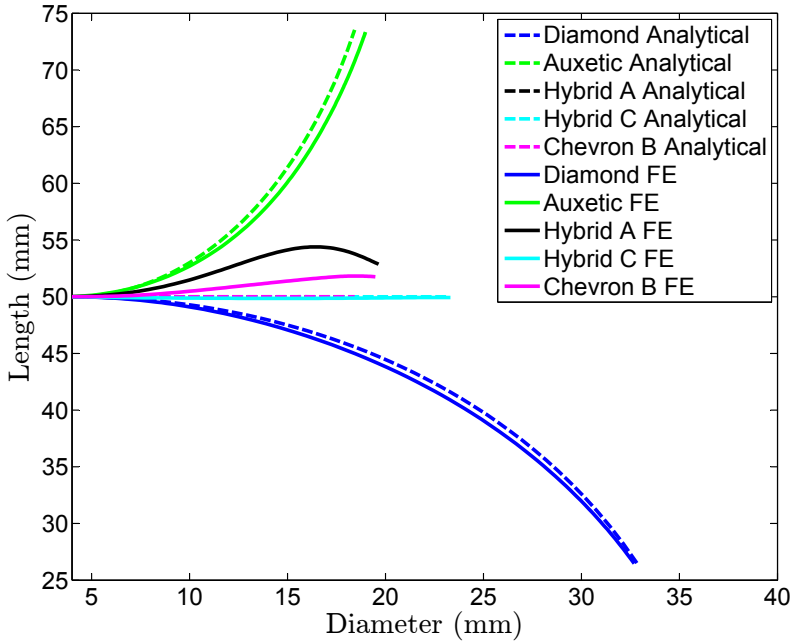

Figure 3.15: Length-diameter relations for the Reid-Reddy and FE methods.

under the 10.7 kPa/ 16.0 kPa physiological-equivalent pressure used here. The stents were from an assumed expanded geometry: expansion itself was not modeled. The material model is different between the studies. Finally, Tan et al. used a constant number of circumferential cells; strut expansion angles to form regular geometric shapes (ie. 45 degrees for Diamond, 30 degrees for Hexagon designs); and a variable strut length. In contrast, the present study used constant strut lengths, a set number of circumferential cells according to a controlled strut thickness, and used variable strut expansion angles to reach the same target diameter.

As such, the mechanical properties of each of these stents should be different in scale, but general features such as relative magnitude of compliance and foreshortening between stent designs should be qualitatively compara-

ble.

Figure 3.16 and Figure 3.17 show the foreshortening and compliance predicted by Tan et al. The Diamond stent foreshortens substantially, the Auxetic design elongates substantially, the Hybrid A design elongates slightly, and the Hybrid C design has negligible axial strain. In magnitude, the axial strain of the Diamond stent is predicted to be about three times the magnitude of the Auxetic stent's strain.

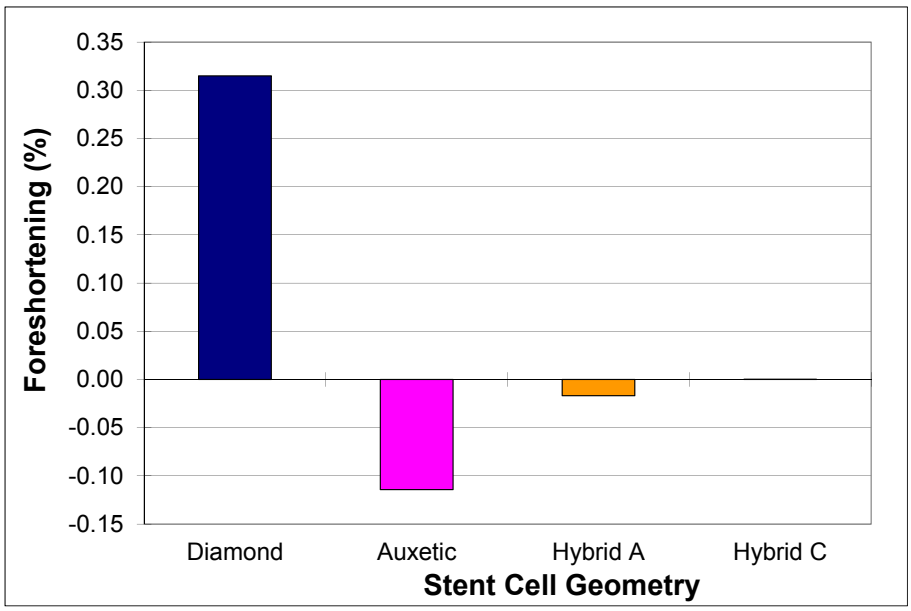

Figure 3.16: Summary of axial strain for various cell geometries, adapted from from Tan et al.

The present study had similar findings, except the magnitude of strain for the Auxetic stent was slightly more than the Diamond stent. This could be attributed to the fact that in the present study, the Diamond cells are expanded to a much lower strut angle than in the Tan et al. study. Thus, changes in diameter will result in a relatively less change in stent length.

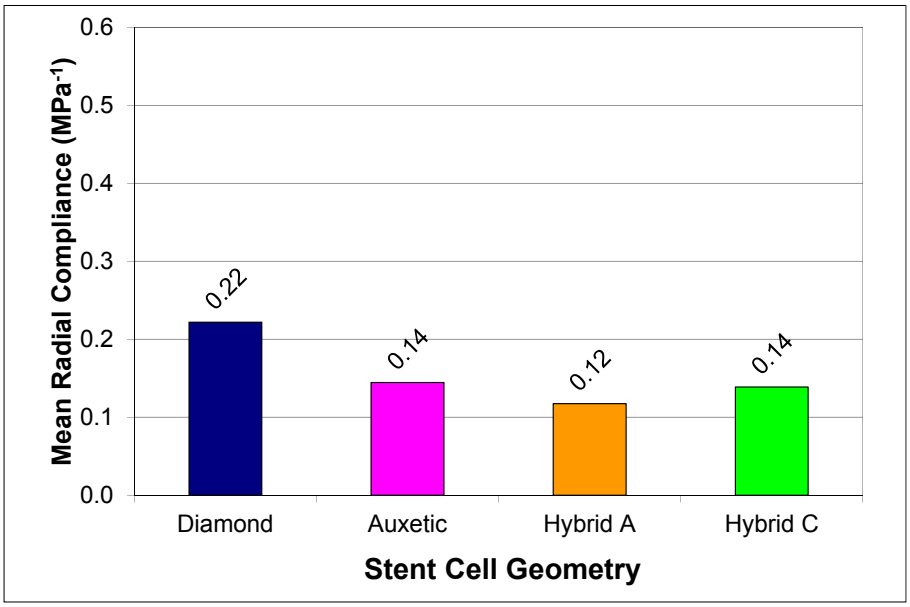

Figure 3.17: Summary of the mean radial compliance for various cell geometries, adapted from from Tan et al.

There are a number of other differences in parameters between the two studies that may also contribute to the difference in relative magnitude of foreshortening of the Diamond stent between the studies.

The absolute magnitude of foreshortening is also about a factor of ten less in the present study than in Tan et al. This is interesting since foreshortening is a non-dimensional parameter and would be expected to be somewhat immune to scale. However, the stiffness (or compliance) of the stents in the two studies is not scaled, so this may contribute to the reduced strain even with the same loads applied.

For compliance, Tan et al reported similar compliances for the Auxetic (0.14 MPa^{-1}), Hybrid A (0.12 MPa^{-1}), and Hybrid C (0.14 MPa^{-1}). The

Diamond design (0.22 MPa^{-1}) is more compliant. The current study found a similar compliance for Auxetic (0.047 MPa^{-1}) and Hybrid A (0.043 MPa^{-1}), a higher compliance for the Hybrid C design (0.082 MPa^{-1}), and higher still for Diamond (0.15 MPa^{-1}).

While there are significant differences in the modeling of these two studies, it is reassuring that the resulting compliances are on the same order of magnitude. Patterns are also preserved through the studies: the Diamond design is most compliant in both studies, and the Auxetic and Hybrid A designs both have similar and the lowest compliances in both studies.

3.5.5 Limitations and Future Work

Given the deviation in the Hybrid A and Chevron B designs from expectations, further modeling is justified. It has been shown in the literature [34] that using a balloon-stent contact model offers improved accuracy over the pressure-stent simulation model used here. Hopefully, a balloon-stent model would give improved certainty over the length-diameter results for the Hybrid A and Chevron B stents. Further, the stent designs that were not tested due to an assumption of being similar to other designs (for example, Hexagon and Double Hexagon being similar to Diamond) should be studied in FE to see if they have unexpected expansion phenomenon.

For these FE models, Cartesian coordinates were used. In future models, using cylindrical coordinates may be preferred. This would allow FE of stent designs that do not have two, orthogonal axes of symmetry. Currently, orthogonal axes of symmetry allow for the required displacement boundary conditions to be applied without complex boundary condition functions.

In addition to the balloon, the artery's geometry should be considered also as a contact model. Arteries in need of stenting rarely, if ever, are straight and having a constant diameter. This creates a complex contact model, creating stresses in both the stent and artery. Blood pressure loading on a stent-artery model may result in greater strains than loading on the stent itself.

An improved plasticity model should be used that better captures the

post-yield behavior than the perfectly-plastic model used here. 316L can vary significantly in its plastic behavior depending on composition, rate of loading, and any heat treating. For the purposes of this study, this complexity was neglected to allow focus on a comparison of unit cell designs, rather than attempt to perfectly model the physics of stenting.

3.6 Conclusions

This chapter presented the Finite Element computational analysis of stent expansion mechanisms. Good agreement with the simpler analytical models in Chapter. 2 is found for the expansions length and diameter characteristics. The next chapter presents experiments on a selected set of stent designs emerging from this and the previous chapter.

Chapter 4

Experiments of Stent Expansion

4.1 Introduction

Computational methods are cheaper and quicker than prototype testing, but lack certainty as no model can completely replicate the physics of the real world. Accordingly, experiments are used to validate portions of the computational study. The intention is to prove that if the computational models have a reasonable match to the physical reality for some parameters, the computational models become validated for use in other simulations with improved certainty.

Three stents are manufactured and expanded by a series of increasingly wider balloons. Diameter, length, diametric recoil, and axial recoil are measured and plotted for each balloon. These results are compared to the expansion and recoil results attained in earlier chapters through analytical and FE methods. Two additional design considerations are then briefly discussed, which illustrate the complexity of stent design.

4.2 Methods

Stents are manufactured (Lumenous Device Technologies, Sunnyvale, CA, USA) for the Diamond, Auxetic, and Hybrid C designs. These stents were chosen due to being the extreme cases of axial strain found in the FE portion of this study. The Diamond design had axial foreshortening, the Auxetic design had the most axial elongation, and the Hybrid C design had no axial strain with expansion.

The stents are manufactured from the same NX6.0 CAD files as the FE study, with the exception that the manufactured stents are whole models and the FE study used symmetry to consider only one eighth of the full model. 2D drawings (.DXF file type) of the stent geometries are sent to the manufacturer, with the drawing showing the unrolled surface geometry of the stent. Thus, one dimension is the length of the stent, the orthogonal direction is the circumference.

The stents are cut from an annealed 316L stainless steel tube, with a 4.0 mm diameter and 0.4 mm wall thickness. The annealed condition is important; for these designs non-annealed stents were found to be stiffer and often punctured the expansion balloon.

A lathe-like machine cuts the stents: a stationary laser cuts the stock tube as the tube is moved axially and rotated circumferentially [44]. The laser used to cut the stents has a kerf width of 20 to 100 micron. For the stents manufactured for this study, the tolerances were set to 20 micron, before post-processing.

After cutting, the stents are deburred mechanically and electropolished. Both of these processes remove material, and the amount of removal can be specified. Surface smoothing and burr reduction is important as sharp edges can puncture the expansion balloon. An electropolished surface also can create a passive oxide layer for improved biocompatability.

The stents are expanded by a series of increasing diameter expansion balloons, with the diameter and length after each step measured with digital calipers and recorded. The balloons used were 9 mm, 10 mm, 12 mm, and 20 mm. The intention was to create experimental data to compare with the length-diameter relation obtained from analytical and FE studies (in Chapter 2 and 3). For some of the balloons, the stent is expanded several times with the balloon at different axial locations within the stent as the balloon is shorter than the stent.

The diameter and length is measured for the stent pressurized by the balloon and the unpressurized, relaxed stent. This allows recoil at each nominal diameter to be calculated. For instances when the stent is longer than the balloon, the measurement of the pressurization state is conducted

with the balloon centered within the stent.

A second Auxetic stent was expanded with only a 9 mm and 20 mm balloon to investigate an interesting buckling pheonomenon that developed in this stent design due to constraints imposed by the balloon-stent interaction. Liquid dish detergent was used in the second Auxetic trial on the balloon to attempt to reduce friction between the stent and balloon.

4.3 Results

Balloon	Diamond		Auxetic		Hybrid C	
Diameter	Diameter	Length	Diameter	Length	Diameter	Length
9 mm	9.82	49.64	9.11	52.24	9.24	50.01
10 mm	10.16	49.32	10.31	53.25	10.24	50.10
12 mm	12.25	48.55	12.07	55.77	12.17	49.98
20 mm	20.10	42.91	19.14	69.17	20.29	50.03
25 mm	25.81	38.54				

Table 4.1: Experimental Diameters (mm) and Lengths (mm) Under Balloon Pressure.

The diameters and lengths of the stents after balloon inflation are presented in Table 4.1. All stents start with a 50.0 mm length and a 4.0 mm diameter. In all cases except the Auxetic stent with the 20 mm balloon, the pressurized stent diameter is greater than the balloon diameter alone. This is expected as the balloon should expand to near its maximum diameter when expanding a stent, and the stent around it has some thickness. The Auxetic stent was predicted in FE and the analytical calculations to have a maximum diameter of about 19 mm.

The post-recoil diameters, shown in Table 4.2, are in all cases less than the initial diameters. The lengths recoiled in such a way as to return towards the original length of 50 mm, with the exception of the Diamond stent after the 9 mm balloon. However, the axial recoil in that trial is so small that the increase could be attributed to measurement error.

Figure 4.1 reports the diameter and length of the three experimentally

Balloon Diameter	Diamond		Auxetic		Hybrid C	
	Diameter	Length	Diameter	Length	Diameter	Length
9 mm	8.52	49.58	8.82	51.87	8.92	50.01
10 mm	9.48	49.56	9.75	52.83	9.46	49.98
12 mm	11.49	48.90	11.57	54.19	11.76	49.94
20 mm	19.40	45.20	19.07	68.58	19.94	50.01
25 mm	24.97	38.55				

Table 4.2: Post-Recoil Experimental Diameters (mm) and Lengths (mm).

tested stents, superimposed on the FE results. The diameters and lengths are for the paths of expansion, including each recoil step. Similar trends are noted in both the FE and Experiments: the Diamond foreshortens, the Hybrid C has no axial strain, and the Auxetic design has axial elongation with expansion.

The curves generated by connecting the experimental data points linearly match the FE curves quite well, with the exception of the Auxetic design at high strain. Here, the diameter exceeds the maximum predicted diameter but the stent does not elongate as much as was expected.

The recoil only partially matches FE. In FE, the Diamond and Auxetic plots did not show hysteresis when recoiled. In the experiments, the stents appear to have relatively more length than diameter recoil compared to FE.

The pre-expanded stents are shown in Figure 4.2. From left to right, they are the Diamond, Auxetic, and Hybrid C designs. The stents are all 4.0 mm in diameter and 50.0 mm long.

The stents after expansion are shown in Figure 4.3. Auxetic [A] is expanded with multiple steps, as according to the protocol stated in the Methods portion of this chapter (p.84). While expanding, it was noted that the ends of the balloon expanded wider than the stent, and constrained the stent from elongating. This axial constraint prevented the Auxetic stent from elongating as much as FE had predicted. Further, this constraining caused buckling of the center on the stent. The axially running struts in the buckled zone, which were predicted not to undergo any rotation while

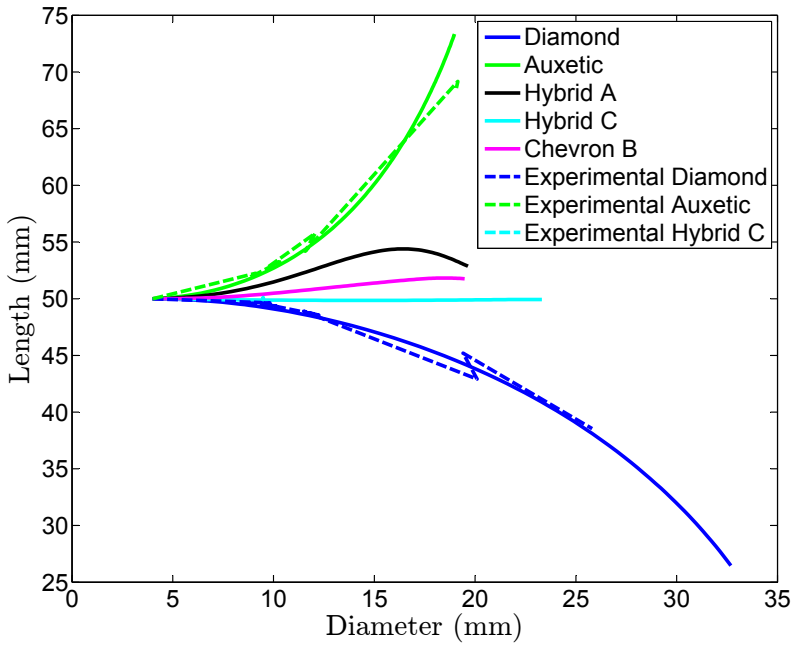

Figure 4.1: Experimental length-diameter relation, compared with the FE results.

the stent expands, have actually undergone a rotation nearly as large as the bending struts.

To further probe this, a second Auxetic stent was expanded using only the 9 mm and 20 mm balloon. It was observed that, since the Auxetic [B] stent was at a smaller initial diameter and length when the 20 mm balloon expansion started, the ends of the balloon constrained the stent from elongating even more. In this stent, two buckling zones have formed. The expansion and recoil data for the Auxetic [B] stent is shown in Table 4.3.

Interestingly, the expanded Auxetic [B] stent has a similar diameter to the Auxetic [A] stent, but is almost 10 mm shorter due to increased buckling. Furthermore, the Auxetic [B] stent was the only observed data point to have

Figure 4.2: The three stents used in the experiments, Diamond (left), Auxetic (middle), and Hybrid C (right).

a *negative* diametric recoil. The axial recoil was in the same direction as the Auxetic [A] stent, but had much more magnitude (1.95 mm compared to 0.59 mm).

The recoil of the stents (excluding Auxetic [B]) at each stage of expansion is compared in Figure 4.4. Similar to the FE data, there does not appear to be much design advice that can be taken from this analysis. There is an indication that the Diamond stent has more recoil, and that stents recoil less as they achieve larger diameters and their strut angle increases.

While expanding the stents, an interesting phenomenon was observed on the Diamond Stent. When the balloon is shorter than the stent, an anti-dogbone effect is formed at the edges (see Figure 4.5). A dogbone effect is

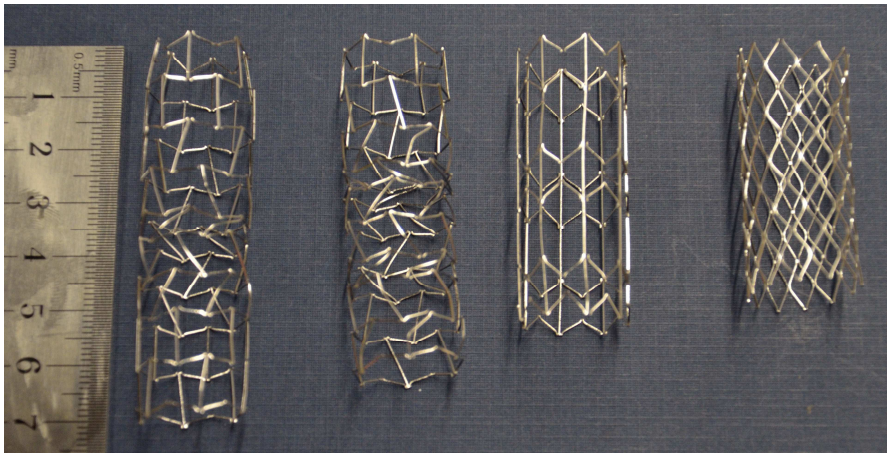

Figure 4.3: The expanded stents after the experiments, Auxetic [A] (left), Auxetic [B] (left-middle), Hybrid C (right-middle), and Diamond (right).

the outward flaring of the stent at the ends, and is clinically observed. It creates a stress concentration at the ends of the stent, which may reduce risk of migration but also leads to higher local stresses in the artery. Anti-dogbone is the reverse: the ends of the stent are under-expanded. This finding confirms the result anticipated by FE analysis of Ju et al. [32].

Anti-dogbone was also observed with the Auxetic stent, but Hybrid C seems more immune. A slight dogbone effect was observed on the Diamond stent using the 20 mm balloon. We have observed larger dogbone effects with the Diamond stent using different expansion protocols.

Balloon Diameter	Auxetic			
	Expanded		Recoil	
	Diameter	Length	Diameter	Length
9 mm	9.16	51.74	8.69	51.56
20 mm	19.51	60.96	19.60	59.01

Table 4.3: The Auxetic [B] Stent Length (mm) and Diameter (mm), for Expansion and Recoil.

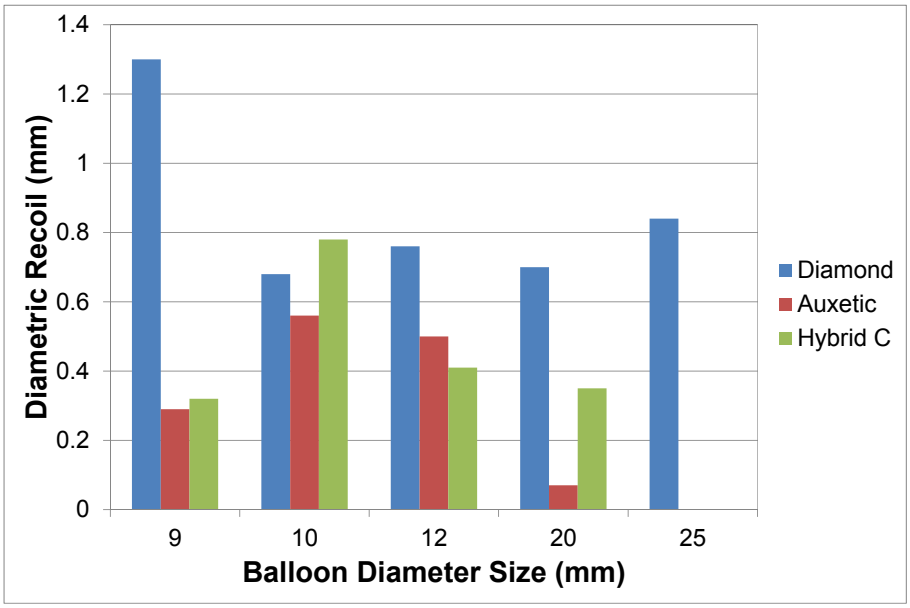

Figure 4.4: Recoil of the three stents for each of the balloons sizes used.

4.4 Discussion

The length-diameter relation of the experiments has reasonable agreement with the finite element prediction, except for the Auxetic stent due to the observed buckling phenomenon. Even if the FE model was altered to in-

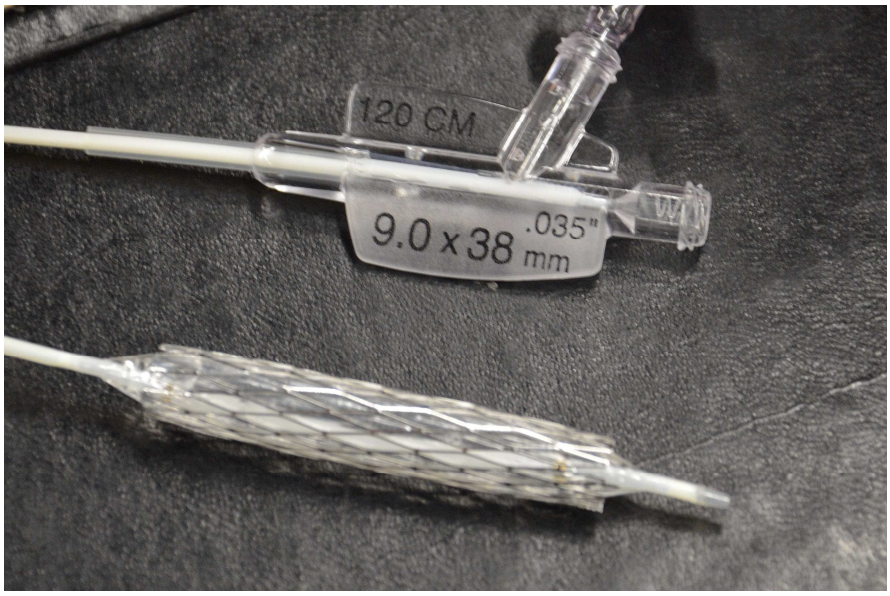

Figure 4.5: A Diamond Stent inflated with a 9 mm diameter x 38 mm length balloon.

clude a balloon as was recommended in the FE chapter, it is still unlikely that a contact model would have predicted the buckling without intentionally including the phenomenon in the model. This highlights that while computational methods are helpful in stent design, it is necessary to include all relevant physical phenomenon in the model. Experimental prototypes continue to be required until the designer is sure the computation model can capture all important mechanisms.

The stents were expanded in air, whereas surgically used stents interact with blood and the vessels. Blood may offer some lubrication to reduce stent-balloon friction, and blood pressure may serve to reduce the amount of over-expansion of the balloon outside the the stent region. With this,

perhaps the Auxetic stent would be less constrained and would be less prone to buckling.

This finding is further evidence against the use of stent designs with large axial strains during expansion, especially elongating strains. Potentially, this elongation could also happen against the artery during expansion, which might provide large stretching and tearing loads. Further investigation is needed if the Auxetic stent is to have a potential clinical use.

Alternatively, balloon coatings could be used to reduce friction of the stent and balloon. Dish detergent was tried in the Auxetic [2] test, but did not stop the stent from being axially constrained by the balloon and did not appear to alter the mechanics at all. Also, the balloon could be designed to reduce risk that the ends of the stent could be constrained. One potential way to do this would be to taper the ends of the balloon inward, so that ends of the balloon can not over-expand. As another alternative, the balloon could axially stretch with the stent, or be constrained in some way so the middle expands before the ends.

The recoil of the Auxetic [B] stent is interesting as it recoiled slightly outwards after expansion with a 20 mm balloon. It also had a very large axial recoil. Recall that this is the test where the axial constraint was largest, and two buckling zones were observed. As the stent was constrained, the loading is no longer just in the radial direction. Further, the buckling that occurred means that the post-expanded stent is no longer a periodic structure. This makes analysis of these phenomenon difficult. The amount of outward recoil is quite small, probably within the measurement error, but even zero recoil would be an interesting finding.

Similarily, in the FE-based recoil results, the recoil of the stent found experimentally doesn't seem to correspond to any pattern that could be attributed to that design. In the FE simulation, the Auxetic design had the least recoil and Hybrid C had the most. In the experiments, the Auxetic design also had the least recoil in most trials, but the Diamond design had the most recoil. It would be interesting to use multiple specimens of the stent to test repeatability of the recoil data. It is possible that some of the differences here could be attributed to experimental variability.

The combined results for the modified pin-jointed, Reid-Reddy, finite element, and experimental methods are shown in Figure 4.6, 4.7, and 4.8. Generally, the match between methods is similar, with deviation for the Auxetic design at high strains where buckling occurs. Note that the axis scales change by figure; for example, the Hybrid C design has a very small y-axis range.

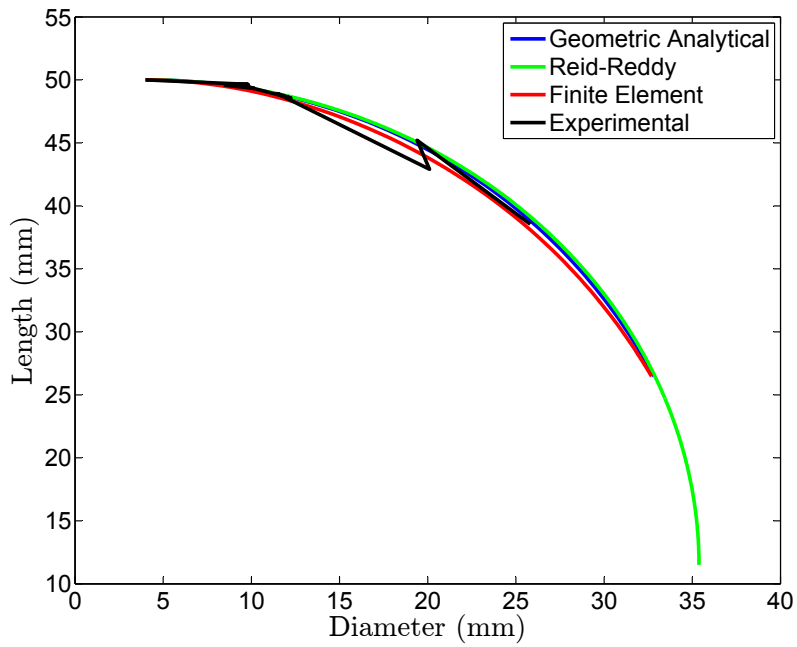

Figure 4.6: The length-diameter relation for all methods for the Diamond stent.

Interestingly, it does not appear that the Diamond stent is much effected by not considering the balloon in the model, but the Auxetic design is highly effected due to the buckling described earlier.

Experimental testing of stent is not without limitations. The small size of the stent makes it difficult to measure stresses in the struts experimentally. The pressure expanding the stent is difficult to measure, as the pressure of

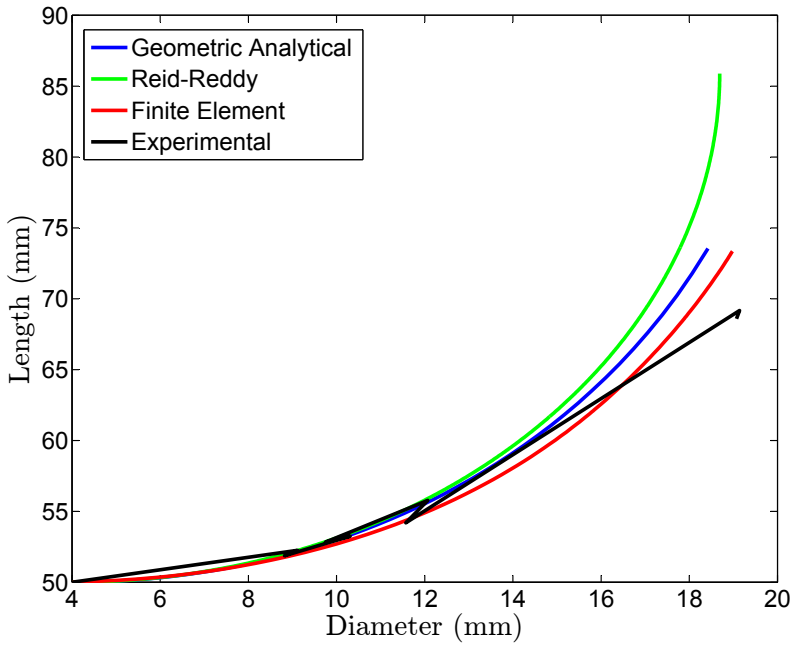

Figure 4.7: The length-diameter relation for all methods for the Auxetic stent.

the fluid in the balloon expands both the balloon and stent simultaneously; it is difficult to separate components. Additionally, the expansion fluid is dynamic: any pressure gauge could not fully account for viscous forces and pressures that unfold the crimped balloon inside the stent. The displacements expected under in vivo loading here are so small (approx. 10 micron over 50 mm) as to be difficult to measure experimentally. Computational methods are better suited for the analysis of these small strain results. As a final point, experimental testing is more expensive and takes longer to get results than computational methods.

Tables 4.4 and 4.5 show the verification process for the various computational methods against experiments. When possible, the diameter and length data from computational methods is linearily interpolated to cor-

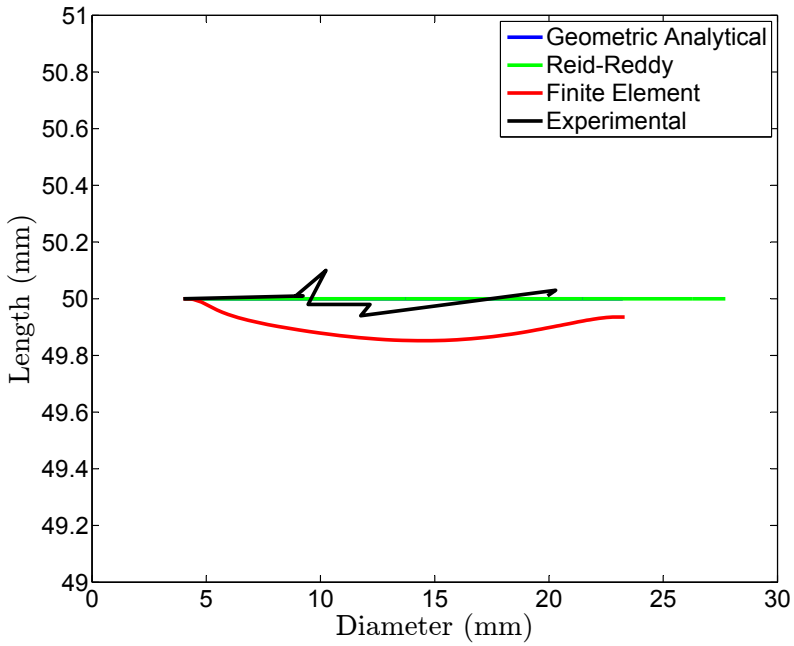

Figure 4.8: The length-diameter relation for all methods for the Hybrid C stent.

respond with a diameter for an experimental data point. The length and difference in length from the crimped state is reported. Finally, the percent error from of the computational change in length data compared to the experimental data is compared.

The exception is the data from the 20mm diameter balloon with the Auxetic stent, for which the experimental data point's diameter exceeded the maximum diameter predicted by the computational methods. For these, the maximum diameter data point is used for diameter and length.

In general, the computational methods match experiment quite well, with the exception of the Auxetic stent with the 20mm diameter balloon. Further optimumization of the methods is possible, for example by improving the material models used in the computational methods. In this study

no optimumization was performed, material and other values were simply taken from the literature. The Auxetic stent had a poor match because the buckling phenomenon was not present in the computational models and a different maximum diameter was predicted in different methods. As the length-diameter curves become vertically assymtotic, the length prediction for a given diameter becomes highly variable with slight changes in diameter. At these points, comparison of relative error of diameter for a given length would give lower errors.

Hybrid C was not included as the axially running members make the error zero in all cases.

	Diameter	Length(mm)	Δ L	Δ L Error (%)
Experiment	10.16	49.32	-0.68	-
FE	10.16	49.30	-0.70	2.34
Reid-Reddy	10.16	49.24	-0.76	12.12
Modified Pin-Jointed	10.16	49.26	-0.74	9.25
Experiment	20.10	42.91	-7.09	-
FE	20.10	43.75	-6.25	11.87
Reid-Reddy	20.10	44.38	-5.62	20.78
Modified Pin-Jointed	20.10	44.55	-5.45	23.14
Experiment	25.81	38.54	-11.46	-
FE	25.81	38.11	-11.89	3.79
Reid-Reddy	25.81	38.83	-11.17	2.57
Modified Pin-Jointed	25.81	39.16	-10.84	5.40

Table 4.4: Error tabulation for the various methods for the Diamond stent.

4.5 Additional Design Considerations

In addition to the design parameters tested here, there are additional design parameters to consider. First is axial flexibility, which describes the ease with which a stent can bend. This is important to allow the stent to be able to tract through tortuous arteries. In general, having larger gaps between stent struts will increase axial flexibility. For instance, the Double Hexagon

	Diameter	Length(mm)	Δ L	Δ L Error (%)
Experiment	10.31	53.25	3.25	-
FE	10.31	52.99	2.99	8.01
Reid-Reddy	10.31	53.33	3.33	2.60
Modified Pin-Jointed	10.31	53.47	3.47	6.80
Experiment	19.14	69.17	19.17	-
FE	18.98	73.35	23.35	21.80
Reid-Reddy	18.42	73.54	23.54	22.80
Modified Pin-Jointed	18.67	85.88	35.88	87.19

Table 4.5: Error tabulation for the various methods for the Auxetic stent.

design would be expected to have improved axial flexibility over the Diamond or Hexagon stent designs.

Prolapse potential is also an important parameter. Unsupported regions of the artery can drape back into the lumen of the artery, reducing cross-sectional area for flow. Garasic et al. have found that, in the absence of injury, a major predictor of final lumen is the gap distance between struts in the cross-section of the stent [45]. However, there is also support of the arteries that comes from stent struts that may be axially located from a particular point on the artery. Therefore, an improved parameter that could be used is the unsupported distance that a point on the artery is from any stent strut.

For this purpose, smaller gap sizes between struts is preferred. Therefore, as a first order model, this design parameter is in direct conflict with the axial flexibility parameter. More thorough analysis, perhaps by FE, is required for these parameters.

4.6 Conclusions

The experiments have provided validation of the computational methods used to analyze the expansion mechanics of stents. There is good agreement between the two analytical methods, the FE method, and the experimental method for the length-diameter relation through the expansion of stents.

The recoil parameter for the stents tested experimentally showed partial agreement with the recoil from FE. It remains uncertain what aspects of the design of stents effect recoil.

A buckling mechanism was discovered from the Auxetic stent being constrained by the balloon during expansion. However, it did not seem that the Diamond stent was effected by axial forces between the stent and balloon since the length-diameter relation from experiment matched the computational methods where the balloon was not modeled.

Chapter 5

Conclusions

5.1 Summary of Present Work and Major Findings

This thesis is concerned with the analysis and design of stent expansion mechanisms based on the principles of lattice mechanics. Certain lattice phenomenon, such as effective Poisson ratio, have been verified to extend from the linear elastic zone to the plastic zone. Plastic mechanics of some lattice designs are presented here for the first time. Further, plastic analysis techniques that greatly simplify behavior prediction have been presented. Plastic analysis of structures is generally considered time consuming and uncertain due to the material and geometric non-linearities involved. Here, two analytical models were presented that can rapidly give insight into different topological designs of stent cells. These methods are found to be in reasonable agreement with more time-consuming FE calculations and experimental results.

The structure of this thesis forms a recommended design process for stents. First, candidate designs can be identified rapidly from many possible geometries using the analytical models presented here. Then, FE studies on promising designs can be undertaken to confirm intended designs. Finally, experimental prototyping should be performed in order to confirm mechanics in the physical world. The advantage of this order is that stents can be tested rapidly in less confident methods to be able to test many more candidate designs in less time. Once the analytical model has been further proven, it may be possible to eliminate the FE step to further save design time.

Several lattice based stent designs were analyzed as candidate starting

designs for stents. Some of these designs have been used as stents previously, some are from lattice literature, and some are created for this study. The main parameters studied were the axial strain with expansion; the compliance of the stent during expansion; maximum expandable diameter; recoil of the stent when the expansion balloon is deflated; axial strain under blood pressure loading; and compliance under blood pressure loading. Additionally, there are other design criteria such as axial flexibility, prolapse potential, strut thickness, and optimal strut length that were mentioned or discussed but not analyzed. Combined, this creates a difficult design problem; hence, the approach of starting with selecting promising unit cell designs.

Even in selecting a unit cell, it is difficult to designate a single design as being best. The Hybrid A and Chevron B designs are promising since they have low axial strain and are axially flexible. However, they also have low strut packing efficiency so they have a relatively low maximum expansion diameter. This may not be an issue for most vessels, but could be for larger vessels such as the aorta. The Diamond cell has efficient strut packing so it has a large maximum diameter and low compliance, but it has significant foreshortening through expansion. This makes accurate placement difficult and potentially has implications for stent-artery interaction.

Both the axial strain and compliance of stents were found to be highly dependent on unit cell choice, but also experience large, non-linear changes with degree of expansion. Presumably, this means that strut length and target diameter are also an important parameters as they affect strut expansion angle.

Recoil was found to be a difficult parameter to compare and analyze, although it is an important design consideration. There was only weak agreement between FE and experimental results, and the experimental results did not have consistency between designs for different expansion diameters.

An interesting buckling phenomenon was observed in the expansion of the Auxetic design. This finding serves in part a two fold caution. First, a caution against relying solely on computational methods to analyze mechanics unless all important mechanisms are accounted of in the model. Second,

a caution against stent designs with large, elongating axial strains without altering balloon designs as these designs are prone to buckle and puncture the balloon.

Some major contributions of this work were:

1. The invention of two analyical models describing the expansion of stents, and expandable structures in general.

2. Experimental confirmation of the anti-dogbone effect predicted by Ju et al. [32].

3. Validation of the two analytical models as well as a finite element model by experiments.

In summary, the research objectives were fulfilled as follows:

1. Two analytical models were developed to efficiently predict expansion behavior of stents.

2. Geometries were designed having a variety of expansion characteristics. Use of the model allows for improved command over parameters effecting stent expansion.

3. The analytical models were validated through FE modeling, which is a technique that has been used multiple times to aid stent design. Both the analytical and FE models were further validated through experimental testing.

5.2 Limitations and Future Work

The analytical and finite element computational models presented here are limited in that they did not include balloon-stent interaction. Experimentally, balloon-stent friction was seen to be small in the Diamond stent, but the contact interaction played a critical role in buckling the Auxetic stent. Later models should capture this behavior if the Auxetic stent is to be further considered a candidate design.

An analytical based prediction of compliance and the pressure-diameter relation was proposed, but issues remain with it so this part of the project has been delegated to future work. Documentation of the proposed approach is in Appendix A. Compliance through expansion is a parameter of limited clinical benefit, so the work presented here does not suffer from this model not being included.

The anatomy the stent is being put into is entirely neglected in this study. At all stages of analysis, the anatomy should be included, ideally in a way to be able to observe and compare stress the various stent designs impose on the artery. Both acute stresses from expansion and long-term stresses from stent-artery interaction are important.

Additional design parameters should be analyzed, to give a more complete understanding of stent mechanics and potentially allow for optimization of stent design. For this, the effect of strut length, strut thickness, and material properties should be further investigated. Further, comparative metrics should be created and analyzed for axial flexibility and prolapse potential for each of the stent designs presented here. The effect of removing select axial struts, as was started with the Double Hexagon design, could complement this analysis.

For the experiments, additional stents should be expanded and measured to offer greater certainty over experimental controls. Additionally, the balloon pressure should be monitored to allow for the calculation of compliance and the pressure-diameter relation for the stents experimentally. The Hybrid A and Chevron B stents should be tested experimentally to observe if they have axial strain, as predicted by FE, or not, as predicted by analytical methods.

5.3 Potential Applications

The analysis techniques and knowledge presented here is most relevant for the design of stents. In some ways, stent design has stagnated after the drug eluting stent revolution that occurred a decade ago. The mechanical design of stents has remained relatively unchanged for even longer. Perhaps

there is an opportunity for a total mechanical redesign of stents, derived from intentional design and optimization of all design parameters. Such a design could be attained from the work presented here complemented with the recommended future work.

In addition to medical devices, there are other deployable structures where lattice-based analysis of plastic structures may be useful. For instance, space payloads and petroleum drilling technologies require highly efficient packing for transit, then reliable, relatively stiff structures at an isolated location. The analysis techniques presented here may have application to technologies in these fields.

Bibliography

[1] Gibson, L. J., and Ashby, M. F., 1997. *Cellular solids: structure and properties*, second ed. Cambridge: Cambridge university press.

[2] Phani, A. S., Woodhouse, J., and Fleck, N. A., 2006. "Wave propagation in two-dimensional periodic lattices". *J. Acoust. Soc. Am,* **119**, pp. 1995–2005.

[3] Tan, T., Douglas, G., Bond, T., and Phani, A. S., 2011. "Compliance and longitudinal strain of cardiovascular stents: Influence of cell geometry". *J. Med. Devices,* **5**.

[4] Dollar, A. L., 1994. "Anatomy of the aorta". In *Diseases of the Aorta*, J. Lindsay, ed. Lea and Febiger, Philadelphia.

[5] Kot, P. A., and Angerio, A. D., 1994. "Physiology of the aorta". In *Diseases of the Aorta*, J. Lindsay, ed. Lea and Febiger, Philadelphia.

[6] Lloyd-Jones, D., and et al, 2009. "Heart disease and stroke statistics - 2009 update". *Circulation,* **119**, pp. 480–486.

[7] Sakalihasan, N., Kuivaniemi, H., Nusgens, B., Durieux, R., and Defraigne, J., 2011. "Aneurysm: Epidemiology artiology and pathophysiology". *Stud Mechanobiol Tissue Eng Biomater,* **7**, pp. 1–33.

[8] J.Lindsay, 1994. "Atherosclerosis and medial degeneration". In *Diseases of the Aorta*, J. Lindsay, ed. Lea and Febiger, Philadelphia.

[9] Kent, K. C., and Boyce, S. W., 1994. "Atherosclerosis and medial degeneration". In *Diseases of the Aorta*, J. Lindsay, ed. Lea and Febiger, Philadelphia.

[10] Dollar, A. L., 1994. "Aortitis: Inflammatory and infectious diseases of the aorta". In *Diseases of the Aorta*, J. Lindsay, ed. Lea and Febiger, Philadelphia.

[11] Dotter, C. T., and Judkins, M. P., 1964. "Transluminal treatment of arteriosclerotic obstruction. description of a new technic and a preliminary report of its application". *Circulation,* **30**, pp. 654–670.

[12] Dotter, C. T., 1969. "Transluminally placed coil-spring endarterial tube grafts: long-term patency in canine popliteal artery". *Invest Radiol,* **4**, pp. 329–332.

[13] Dotter, C. T., Buschmann, R. W., and et al., 1983. "Transluminally expandable nitinol coil stent grafting: preliminary report". *Radiology,* **147**, pp. 259–260.

[14] Palmaz, J. C., 1985. "Expandable intraluminal graft and method and apparatus for implanting an expandable intraluminal graft". *US Patent,* **4,733,665**.

[15] Kessel, D. O., 2010. "Basic tools required to preform angioplasty and stenting procedures". In *Handbook of angioplasty and stenting procedures*, R. A. Morgan and E. Walser, eds. Springer-Verlag, London.

[16] Rogers, C., and Edelman, E. R., 1995. "Endovascular stent design dictates experimental restenosis and thrombosis". *Circulation,* **91**, pp. 2995–3001.

[17] Berry, J. L., Manoach, E., Mekkaoui, C., Rolland, P. H., Moore, J. E., and Rachev, A., 2002. "Hemodynamics and wall mechanics of a compliance matching stent: In vitro and in vivo analysis". *J. Vasc. Interv. Radiol.,* **13**(1), pp. 97–105.

[18] Spaulding, C., aemen, J., Boersma, E., Cutlip, D., and Serruys, P., 2007. "A pooled analysis of data compating sirolimus-eluting stents with bare-metal stents". *N Eng J MEd,* **356**, pp. 989–997.

[19] Lagerqvist, B., James, S. K., Stenestrand, U. Lindbck, J., Nilsson, T., and Wallentin, L., 2007. "Long-term outcomes with drug-eluting stents versus bare-metal stents in sweden". *The New England Journal of Medicine,* **356**(10), pp. 1009–1019.

[20] Kastrati, A., Mehilli, J., Dirschinger, J., Pache, J., Ulm, K., Schhlen, H., Seyfarth, M., Schmitt, C., Blasini, R., Neumann, F. J., and Schmig, A., 2001. "Restenosis after coronary placement of various stent types". *Am J Cardiol,* **87**, pp. 34–39.

[21] Kastrati, A., and Dirschinger, J. e. a., 2000. "Influance of stent design on 1 year outcome after coronary stent placement: A randomized comparison of five stent types in 1,147 unselected patients". *Catheterization and Cardiovascular Intervention,* **50**, pp. 290–297.

[22] Hara, H., Nakamura, M., Palmaz, J. C., and Schwartz, R. S., 2006. "Role of stent design and coatings on restenosis and thrombosis". *Adv. Drug. Deliv. Rev.,* **58**, pp. 377–386.

[23] Moore, J. E., and Berry, J. L., 2002. "Fluid and solid mechanical implications of vascular stenting,". *Annals of Biomedical Engineering,* **30**, pp. 498–508.

[24] Holzapfel, G. A., Stadler, M., and Gasser, T. C., 2005. "Changes in the mechanical environment of stenotic arteries during interaction with stents: Computational assessment of parametric stent designs". *Journal of Biomechanical Engineering,* **127**, pp. 166–180.

[25] Tan, L. B., Webb, D. C., Kormi, K., and Al-Hassani, S. T. S., 2001. "A method for investigation the mechanical properties of intracoronary stents using finite element numerical simulation". *Int. J. Cardiol.,* **78**, pp. 51–67.

[26] Charalambides, A., 2011. "Modeling of the balloon-stent-vessel expansion mechanics". *University of Maryland Masters Thesis*, pp. 1–201.

[27] Zahora, J., Bezrouk, A., and Hanus, J., 2007. "Modeling of stents - comparison and applications". *Phsiol. Res.,* **56 (Suppl. 1)**, pp. S115–S121.

[28] Lally, C., Dolan, F., and Prendergast, P. J., 2005. "Cardiovascular stent design and vessel stresses: A finite element analysis,". *Journal of Biomechanics,* **38**, pp. 1574–1581.

[29] Bedoya, J., Meyer, C. A., Timmins, L. H., and Moore, J. E., 2006. "Effects of stent design parameters on normal artery wall mechanics,". *J. Biomech.,* **128**, pp. 757–767.

[30] Petrini, L., Migliavacca, F., Auricchio, F., and Dubini, G., 2004. "Numerical investigation of the intravascular coronary stent flexibility". *Journal of Biomechanics,* **37**, pp. 495–501.

[31] Mori, K., and Saito, T., 2005. "Effects of stent structure on stent flexibility measurements". *Annals of Biomedical Engineering,* **33(6)**, pp. 733–742.

[32] Ju, F., Xia, Z., and Sasaki, K., 2008. "On the finite element modeling of balloon-expandable stents". *Journal of the Mechanical Behavior of Biomedical Materials,* **1**, pp. 86–95.

[33] Wang, W.-Q., Liang, D.-K., Yang, D.-Z., and Qi, M., 2006. "Analysis of the transient expansion behavior and design optimization of coronary stents by finite element method". *J. Biomech,* **39**, pp. 21–32.

[34] Beule, M. D., Mortier, P., Carlier, S., Verhegghe, B., Impe, R. V., and Verdonck, R., 2008. "Realistic finite element-based stent design: the impact of balloon folding". *J. Biomech,* **41**, pp. 383–389.

[35] Hoffmann, R., Mintz, G. S., Haager, P. K., Bozoglu, T., Grube, E., Gross, M., Beythien, C., Mudra, H., vom Dahl, J., and Hanrath, P., 2002. "Relation of stent design and stent surface material to subsequent in-stent intimal hyperplasia in coronary arteries determined by intravascular ultrasound". *Am J Cardiol,* **89**, pp. 1360–1364.

[36] Sick, P. B., Thiele, H., Brosteanu, O., Hentschel, B., Lauer, B., Neibauer, J., Hambrecht, R., and Schuler, G., 2003. "Prospective radomized comparison of early and late results of 4 different stent designs". *Am. Heart J.,* **146(1)**, pp. 134–141.

[37] Yoshitomi, Y., Kojima, S., Yano, M., Sugi, T., Matsumoto, Y., Saotome, M. Tanaka, K., Endo, M., and Kumochi, M., 2001. "Does stent design affect probability of restenosis? *a* randomized trial comparing multilink stents with gfx stents". *Am Heart J,* **142**, pp. 445–451.

[38] Sullivan, T. M., Ainsworth, S. D., Langan, E. M., Tayloe, S., Snyder, B., Cull, D., Youkey, J., and Laberge, M., 2002. "Effect of endovascular stent strut geometry on vascular injury, myointimal hyperplasia, and restenosis". *J Vasc Surg,* **36**, pp. 143–149.

[39] Baker, J. F., 1954. *The Steel Skeleton*, first ed. Cambridge: Cambridge university press.

[40] Chopra, P., 2011. "Effective properties of lattice materials". *UBC MASc Thesis.*

[41] Reid, S. R., and Reddy, T. Y., 1978. "Effect of strain hardening on the large plastic deformaton of a cantilever". *J. Appl. Mech.,* **45**, pp. 953–955.

[42] Levesque, J., Dube, D., Fiset, M., and Mantovani, D., 2004. "Materials and properties for coronary stents". *Advanced Materials & Processes*, pp. 45–48.

[43] Chua, S. N. D., MacDonald, B., and Hashmi, M. S. J., 2002. "Finite-element simulation of stent expansion". *J. Mater. Proc. Technol.,* **120**, pp. 335–340.

[44] Technologies, L. D., 2012. Lumenous device technologies website. http://www.lumenous.com/.

[45] Garasic, J. M., Edelman, E. R., Squire, J. C., Seifert, P., Williams, M. S., and Rogers, C., 2000. "Stent and artery geometry determine intimal thickening independent of arterial injury". *Circulation*, pp. 812–818.

Appendix A: Future Work on Analytical Compliance

Another advantage of the Reid-Reddy method is that the formulation is not purely geometrical: it does account for loading on the struts and thus the comparative stiffness of the stents during expansion can be predicted.

The force-deflection relation is shown in Chapter 2 as Figure 2.8. This relation could be related to a pressure-diameter relation through geometry and equating work.

Consider a unit strut, where the unit consists of one cantilever that bends as well as non-bending material, such that the amount of non-bending material at a node is distributed evenly between all struts at that node.

By this stent expansion model, the stent is only loaded by pressure applied to the stent, which is assumed to be constant throughout the stent's inner surface. An increase in pressure causes a change in diameter of the stent, and thus the struts of the stent rotate. The work done by a pressure causing an increase in radius of dr is given by:

$$W = \int PAdr \tag{1}$$

Where P is the pressure, A is the surface area inside the unit strut, and dr is the change in radius of the stent. Similarly, stent expansion work can be considered as an internal Reid-Reddy cantilever force going through a displacement V:

$$W = \int FdV \tag{2}$$

By equating equations for circumference from the radius and stent strut displacement, then taking the derivative, the following expression is attained:

$$\frac{dV}{dr} = \frac{\pi}{2n_c} \tag{3}$$

for all designs except double hexagon, which is

$$\frac{dV}{dr} = \frac{\pi}{4n_c} \tag{4}$$

These equations are combined to find a relation for pressure given the geometry of the stent and the Reid-Reddy force-displacement relation:

$$P = \frac{F\pi}{2n_c A} \tag{5}$$

Figure 1 shows the predicted pressure-diameter relation for six stent designs. All curves have the same general shape, but a different final diameter and yield point.

For the pressure-diameter plot, Appendix Figure 1, the final diameter here is the same as that found in the length-diameter relation, from Figure 2.7 (in Chapter 2). The slope of the plots flattens as it approaches the final diameter, that is the stents become stiffer as they reach their final diameter. This is expected as the struts are becoming loaded more as stretched and less as bending cantilevers. The internal force that causes the stent struts to bend increasingly becomes aligned with the strut and as the strut rotates.

A useful comparison is between the Diamond, Hexagon, and Double Hexagon designs. Recall that the Hexagon is the Diamond design with added axial connectors of one strut length. The Double Hexagon design is the same as the Hexagon, but with alternate axial struts removed. Accordingly, all of these designs have the same number of unit struts within their circumference. Therefore, any difference in performance between the designs is a result of different non-bending areas between each of the unit struts. The results

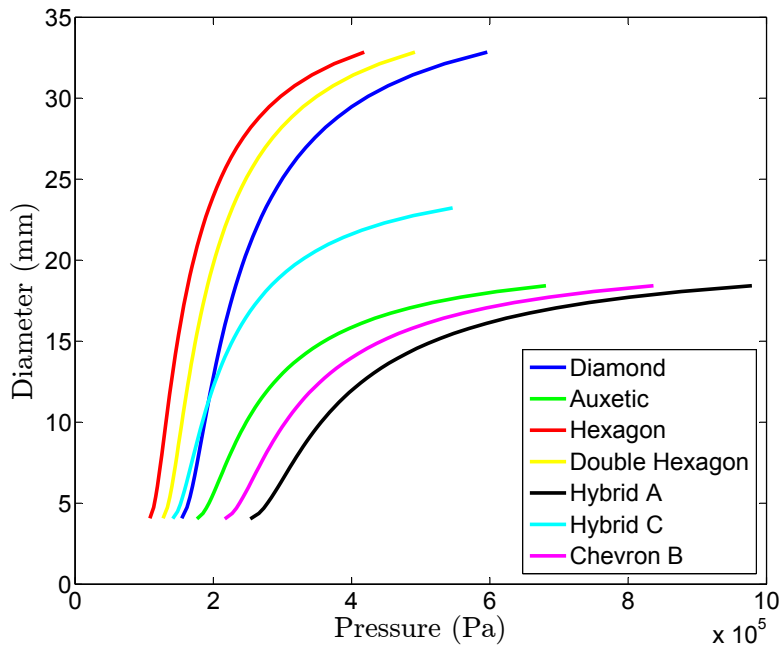

Figure 1: Pressure-diameter relations of the stents modeled as a structure of Reid-Reddy cantilevers.

then do match the results expected from the method of equations above, as the Hexagon has much more non-bending area than the Diamond design, with the Double Hexagon design being between the two.

Similarly, the Auxetic, Hybrid A, and Chevron B designs have the same circumferential number of strut units as well as circumferential number of unit cells. The Auxetic unit cell has one non-bending strut with a length of $2l$; the Hybrid A unit cell has non-bending struts as part of the Hexagon and Auxetic portions of the unit cell as well as a non-bending strut connecting the two sub-cells, but also a relatively open design; and the Chevron B unit cell has one non-bending strut.

The pressure-diameter relation presented here is a model of stent ex-

pansion. It is highly simplified compared to the balloon-stent interaction present in reality. It remains to be seen if having greater non-bending area in contact with the expansion balloon causes a more compliant stent, for instance. The compliances here raise a caution for balloon rupture: the 20 mm diameter balloons we used the the Experiments portion of this thesis have a rating of 7ATM for their burst rating, which roughly corresponds to 700 kPa and is in the range of the results seen here. However, in our experience balloon failure in our experiments the result of the stent puncturing the balloon and not from over-pressurization.

A stiff stent may be more difficult for the surgeon to implant, but there are tools to increase expansion pressures. The approximation of the struts as rectangular cross-sectioned cantilevers introduced error as well, particularly in calculating the bending moment of area and that uses the outer diameter strut length to calculate pressurized area of expansion.

Also to be considered is the linear-elastic compliance of the stent under physiologic blood pressure loading, as the interaction with the anatomy under these conditions may guide remodeling. This analytical model could be expanded in the future to include the recoil of the stent when the expansion balloon is removed as well as the cyclic blood pressure loading.

The pressure-diameter relation for the Reid-Reddy analytical and finite element approaches are reproduced for comparison (see Figure 2).

The pressure-diameter relations also match well for some of the stents. Both methods predict the Diamond being the most compliant. The Hybrid C design has a lower compliance than Diamond, and the Auxetic, Hybrid A, and Chevron B designs have a similar, and lower still, compliance.

The methods do differ in their predictions for initial expansion and yielding. Both predict the stents yield at about 200 kPa, but the Reid-Reddy method predicts a greater spread in yield values. Recall the analytical method assumes a rigid-linear plastic model. The elastic phase is neglected, and the area around the yield point of the stents has a transition between being elastic and fully plastic. It may be possibly to adapt the analytical method to include the fully elastic and elastic-plastic transition phase of expansion. For example, linear elastic analysis of unit cells similar to those

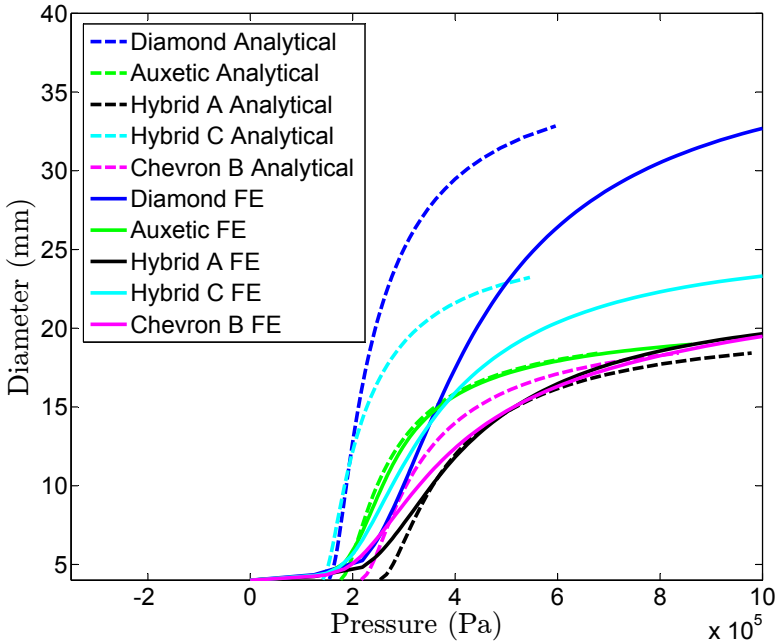

Figure 2: Pressure-diameter relations for the Reid-Reddy and FE methods.

in this study has been performed by Gibson and Ashby [1]. The linear phase could form an initial displacement before the Reid-Reddy method is used, or further there could be some scaling model to transition the fully elastic to the plastic Reid-Reddy model.

The slopes of the Diamond and Hybrid C stents are steeper for the Reid-Reddy version than the FE method. This indicates a lower compliance.

In both the FE and Reid-Reddy method, the area the pressure is on is the inside surface of the stent. In reality, the pressurized area probably corresponds more to the area of the sector of the balloon that loads a stent strut. The Reid-Reddy method is quite sensitive to the area used, as pressurization of non-bending struts is distributed to load bending struts. This should be further investigated and optimized to have a clearer picture of the

model of the mechanics involved.

Stent expansion forces could be idealized as hoop stresses. Thus, in the circumference, expansion forces are the same in all cells and thus all bending struts, assuming all cells are identical and expand at the same rates. Therefore, the yield point should be roughly the same for all stents, irrespective of the number of cells in the circumference. This would explain why the FE stents yield at about the same point, and suggests that the FE result is the correct one. Further investigation is required, and should focus on the Reid-Reddy method for finding the pressure-diameter relation. In particular, there is uncertainty in the formulation used to equate the work to open a Reid-Reddy cantilever and the work the balloon pressure does to expand a strut.

Further work on this model is needed to be confident in its results, but the clinical benefit of the model is probably limited compared to other parameters studied in this thesis.